The Journal of Neuroscience, December 1995, 15(12): 7778–7795

Perisynaptic Surface Distribution of Multiple Classes of Nicotinic Acetylcholine Receptors on Neurons in the Chicken Ciliary Ganglion

Hadley L. Wilson Horch and Peter B. Sargent

Departments of Stomatology and Physiology and the Neuroscience Graduate Program, University of California, San Francisco, California 94143

Most nicotinic ACh receptors (AChRs) studied to date in the embryonic chicken ciliary ganglion are recognized either by monoclonal antibody (mAb) 35 or by α-bungarotoxin (α-Bgt). Previous studies found that mAb 35-AChRs are found at both synaptic and extrasynaptic sites, while α-Bgt-AChRs are found exclusively at extrasynaptic sites. To gain a three-dimensional understanding of the distribution of these two AChR classes and their spatial relationship to synaptic sites, we have visualized mAb 35-AChRs and α-Bgt-AChRs immunofluorescently using laser scanning confocal microscopy and have compared their distribution with that of the synaptic vesicle antigen SV2. Both mAb 35-AChR and α-Bgt-AChRs are found in clusters that are widely distributed over the surface of embryonic chicken ciliary ganglion neurons. Some mAb 35-AChRs are located at synaptic sites, but the bulk of them are located extrasynaptically in well-defined patches measuring 1–4 μm in diameter. α- Bgt-AChRs are found almost exclusively in these extrasynaptic sites, which thus contain both AChR types. These sites are often surrounded by elements of the synaptic calyx but are themselves largely free of SV2 antigen. In 14 week chickens the relationship between mAb 35-AChRs, α-Bgt-AChRs, and synaptic sites is similar to that in embryos except that in this instance individual synaptic boutons are often surrounded by AChR-containing patches. These results suggest that most surface AChRs in both embryonic and mature chicken ciliary neurons are perisynaptic, which raises questions about the function of these AChRs.

[Key words: ACh receptors, α-bungarotoxin, calyx, synapses, extrasynaptic, confocal microscope]

Adult skeletal muscle cells synthesize only one class of AChRs at a time; innervated cells make AChR oligomers having the subunit composition $\alpha_2\beta\epsilon\delta$, while denervated cells make AChRs having the composition $\alpha_2\beta\gamma\delta$ (reviewed in Hall and Sanes, 1993). By contrast, selected neurons can express multiple AChR classes at the same time (reviewed in Sargent, 1993, and McGehee and Role, 1995). The extent of diversity in AChR expression has been best characterized in the chicken ciliary ganglion, where most neurons express a class of AChRs recognized by monoclonal antibody (mAb) 35 and a largely distinct AChR class recognized by α-bungarotoxin (α-Bgt). MAb 35-AChRs contain the α3, α5, β2, and β4 subunits but lack α7 subunits (Vernallis et al., 1993; Conroy and Berg, 1995), while α-Bgt-AChRs contain α7 subunits but lack α3, α5, β4, or β2 subunits (Couturier et al., 1990; Schoepfer et al., 1990; Vernallis et al., 1993). Jacob et al. (1984) and Jacob and Berg (1983) used mAb 35-horseradish peroxidase (HRP) and α-Bgt-HRP to examine, with the electron microscope, the distribution of mAb 35-AChRs and α-Bgt-AChRs on the surface of embryonic ciliary ganglion neurons. mAb 35-AChRs were found at most synaptic sites and were also occasionally associated with small processes ("pseudodendrites") lying adjacent to synaptic sites (see also Loring and Zigmond, 1987). By contrast, α-Bgt-AChRs were found exclusively in extrasynaptic locations and principally in association with small processes (Fumagalli and DeRenzis, 1980; Jacob and Berg, 1983; Loring et al., 1985). MAb 35-AChRs are likely to underlie rapid synaptic transmission in the ciliary ganglion, since (1) they are located at synaptic sites, (2) incubation of cultured ciliary ganglion neurons with mAb 35 downregulates the number of mAb 35-AChRs and reduces ACh sensitivity (Smith et al., 1986), and (3) synaptic transmission and ACh responses elicited from ciliary ganglion neurons are blocked by neuronal bungarotoxin (κ-bungarotoxin) (Ravdin and Berg, 1979; Chiappinelli, 1983; Loring et al., 1984), which recognizes a receptor also recognized by mAb 35 (Halvorsen and Berg, 1987). The function of α-Bgt-AChRs is unclear, inasmuch as these AChRs are extrasynaptic. α-Bgt-AChRs contain α7 subunits (Schoepfer et al., 1990; Conroy et al., 1992; Vernallis et al., 1993) and both heterologously expressed chick α7 homooligomers (Couturier et al., 1990) and chick ciliary ganglion α-Bgt-AChRs have a high calcium permeability (Vijayaraghavan et al., 1992; Zhang and Berg, 1994). The high calcium permeability of α-Bgt-AChRs raises the possibility that they modulate target cell function *in vivo* via calcium entry and calcium-dependent second messenger pathways (Vijayaraghavan et al., 1995). If so, then several questions arise: which pathways operate, what are their natural targets, and under what conditions are α-Bgt-AChRs activated by natural transmitter? To learn more about the conditions under which α-Bgt-AChRs might be activated by natural transmitter, we sought to view, in three di-

Received May 26, 1995; revised July 18, 1995; accepted July 20, 1995.

We thank Drs. Darwin Berg, Steven Carlson, and Jon Lindstrom for antibodies; Drs. Michele Jacob, Ralph Loring, and Patricia Steen for critically reading a draft of the manuscript; Dr. Kent Keyser for perfused chicken heads; Dr. Lauren Ernst for advice on conjugating α-Bgt with cyanine 3.18; and Gordon, James, and Suzanne for pullets. This work was supported by NIH Grants NS 24207 and RR 07131.

Correspondence should be addressed to Dr. Peter B. Sargent, Division of Oral Biology, HSW-604, University of California, San Francisco, CA 94143-0512.

mensions, the distribution of α-Bgt-AChRs in relation to synaptic sites and in relation to the other principal AChR class, mAb 35-AChRs. Our results suggest that most α-Bgt-AChRs and mAb 35-AChRs in both embryonic and adult chick ciliary ganglia are located immediately adjacent to synaptic sites. These AChRs presumably are not involved in mediating fast excitatory synaptic transmission in the ganglion.

These results have been presented previously in abstract form (Sargent and Wilson, 1994).

Methods and Materials

Tissue. White Leghorn chicken eggs were obtained from a local supplier and kept in a forced draft incubator at 39°C. Embryos aged 19–21 d were sacrificed by decapitation, and the ciliary ganglia were rapidly removed in chick Ringer's (144 mM NaCl, 6 mM KCl, 2.3 mM $MgCl_2$, 5.6 mM $CaCl_2$, 5.0 mM HEPES, pH 7.2) and fixed in 0.5% formaldehyde in 0.11 M Na phosphate, pH 7.2, for 1 hr at room temperature (22–24°C). In a few instances, unfixed whole ganglia were incubated with reagents as described by Jacob and Berg (1983) and Jacob (1991). Tissue from 12 week hens was obtained after perfusion of animals with 1.0% formaldehyde in Na phosphate, pH 7.2, and by subsequent immersion fixation, as for embryos. Similar results were obtained on 14 week hens obtained within 15 min of sacrifice at an abattoir and stored on ice for 30 min before dissection and immersion fixation. Whole ganglia were desheathed and cut in half before incubations with reagents. Ganglia to be used for frozen sections were cryoprotected in 30% sucrose in chick Ringer's and frozen in tissue freezing medium before being sectioned at 12 μm in a cryostat and mounted on subbed slides.

Ligands. α-Bgt was obtained from Biotoxins, Inc. (St. Cloud, FL; claimed to be "extremely pure" by SDS PAGE) and conjugated with cyanine 3.18 (Cy3) to a calculated molar dye/protein ratio of 1:1 using a labeling kit (Biological Detection Systems, Pittsburgh, PA). Rat anti-electric organ AChR mAbs 35 (Tzartos et al., 1981), 210 (Tzartos et al., 1987), and 12 (Tzartos and Lindstrom, 1980) were generously provided by Dr. Jon Lindstrom (University of Pennsylvania). Among the AChR subunits known to be expressed in the ciliary ganglion (α3, α5, α7, β2, and β4), only α5 is recognized by mAbs 35 and 210 in immunoblots (Vernallis et al., 1993). MAbs 35 and 210 may recognize either the α5 or the α3 subunit when they are coexpressed heterologously with the β4 subunit (Haselbeck et al., 1994). Mouse anti-SV2 mAb 10h (Buckley and Kelly, 1985) was generously provided by Dr. Steven Carlson (University of Washington) and was conjugated with cyanine 5.18 (Cy5) to a calculated molar dye/protein ratio of 1.3:1 using a labeling kit (Biological Detection Systems, Pittsburgh, PA). All primary mAbs used are IgGs. Conjugated goat anti-mouse and anti-rat secondary antibodies cleaned of conspecific cross-reactivity were obtained from Jackson Immunoresearch, Inc. (West Grove, PA). All other reagents were obtained from Sigma (St. Louis, MO) unless otherwise noted.

Immunofluorescence experiments were performed on frozen sections or on whole mounts of fixed ciliary ganglia using antibody or toxin concentrations diluted in chick Ringer's to a final concentration of 15–30 nM. Nonspecific binding was reduced by "blocking" with 5% normal goat serum (Irvine Scientific, Irvine, CA) in Ringer's, and tissue was mounted in 90% glycerol/10% phosphate-buffered saline containing 4% *n*-propyl gallate (Giloh and Sedat, 1982) and stored at −20°C until examined. Additional details of individual labeling protocols are given below.

Immunofluorescence on frozen sections. For mAbs: block (10 min), primary mAb (30 min), rinse (10 min), secondary antibody (30 min), rinse, mount. For α-Bgt: block (10 min), toxin (30 min), rinse (10 min), mount. All steps done at room temperature.

Immunofluorescence on whole mounts. Blocking was done for 30 min. Antibody and toxin incubation steps were done for 3 hr at room temperature (22–24°C) or overnight at 4°C. Other steps were done at room temperature. In one experiment antibody incubation steps were lengthened to 24 hr at 4°C. Rinsing steps were done for 30 min, with three changes. Permeabilization was done by incubating tissue with 0.3% Triton X-100 in Ringer's for 30 min.

For mAb 35-AChRs versus synaptic sites: block, mAb 35 or mAb 210, rinse, Cy3-goat anti-rat IgG, permeabilize, Cy5-mAb 10h (or mAb 10h followed by Cy5-goat anti-mouse IgG), rinse, mount.

For α-Bgt-AChRs versus synaptic sites: block, Cy3-α-Bgt, rinse, permeabilize, Cy5-mAb 10h (or mAb 10h followed by Cy5-goat anti-mouse IgG), rinse, mount.

For mAb 35-AChRs versus α-Bgt-AChRs: block, Cy3-α-Bgt, rinse, mAb 35 or mAb 210, rinse, Cy5-goat anti-rat IgG.

For triple label: block, Cy3-α-Bgt and mAb 210, rinse, Cy5-goat anti-rat IgG, rinse, permeabilize, mAb 10h, rinse, FITC-goat anti-mouse IgG, rinse, mount.

During a 3 hr incubation Cy3-α-Bgt (MW < 10 kDa) will label cell surfaces heavily through the entire thickness of the whole-mounted ganglion, while molecules the size of IgGs will label cell surfaces heavily only within 50–100 μm of the surface of the ganglion. We therefore analyzed only those neurons lying within 25–50 μm of the ganglion surface: that is, the cortical one to three layers of cells. In a few instances we altered the incubation protocol in ways that resulted in labeling of neurons within the core of the ganglion, either by prolonging the incubation times to 24 hr or by pretreating the ganglia with collagenase (Sigma, type II, 1 mg/ml, 37°C, 30–60 min) and subsequently with subtilisin (Calbiochem, 0.1 mg/ml, 37°C, 15–30 min), as described by Sargent and Pang (1989).

Immunofluorescently stained neurons were visualized using a Bio-Rad MRC-600 laser scanning confocal microscope equipped with filter blocks optimized for Cy3 and Cy5 (Sargent, 1994). To avoid photobleaching Cy5, we usually performed Z-series reconstructions using only the 568 nm laser line, which excites Cy5 with ca. 11% efficiency and is sufficient for most applications. Confocal images are displayed as (1) individual optical sections taken through the middle of neurons, (2) collections of two to four adjacent optical sections taken through the upper or lower surfaces of neurons (hereafter referred as upper surface, for convenience), or (3) stereo pairs generated from reconstructions. Reconstructions were typically performed with a z-increment of 1.0 μm and with the detector apertures set at 3 mm, which yields a measured section thickness of 1.2 μm (568 nm) when using the Nikon 60× 1.4 NA oil immersion planapochromat lens. In a few instances, reconstructions were done with a z-increment of 0.25 μm, to insure that we were not missing essential information. All images were collected with LOW SIG on, with slow scan, and with a scan box of $(384 \text{ pixels})^2$ per channel. For optimal display of images, photomultiplier gain and black levels were adjusted so that a few pixels in the field (≪1%), or anywhere in a stack of fields (for reconstructions), registered 0, a few pixels registered 255, and the remaining pixels registered intermediate values. For comparison of different mAbs (e.g., see Fig. 1) or different incubation conditions, all images from an experiment were collected under identical conditions. Laser intensity was attenuated to 3% or 1% using neutral density filters. All images are displayed with signal averaging but without any filtering or alteration of look-up tables. It is unlikely that we can visualize individual fluorophores or individual AChR molecules with this collection procedure, and we assume that fluorescence signals represent clusters of AChR molecules. The limit of resolution of this system was not measured but is no better than 0.3 μm in the x-y plane and 0.6 μm in the z-axis.

We quantified intracellular signal intensity in frozen sections by collecting images from 10 324 × 216 μm fields and by using the Optimas image analysis program to measure average gray values (pixel intensities) from rectangular areas within the interior of every cell (avoiding the nuclei, which were usually unstained). In a separate analysis, we determined whether individual neurons were specifically labeled on a cell-by-cell basis by setting a threshold for object detection sufficiently high so that few or no cells were labeled in fields of neurons in the control group. This threshold was then applied to neurons in the experimental group; cells were scored as labeled if they had any objects within their interior or on their surface that satisfied threshold criteria.

Neurons were chosen for reconstruction based on two criteria: (1) that they be sufficiently isolated from other neurons (more than 2 μm of separation) to eliminate confusion as to the source of signal, and (2) that they be well stained. Most cells analyzed using these criteria had calyceal endings on them, as judged by the appearance of SV2 immunoreactivity, and were considered to be ciliary neurons (Hess, 1965). Choroid neurons, which have bouton-like endings, were not generally chosen for analysis because they appear to be more densely packed than ciliary neurons. Most or all cells viewed at low power within the cortex of the ganglion appeared to be well-stained with Cy3-α-Bgt or with mAbs 35 or 210, visualized directly or indirectly. However, perhaps one-fifth of the neurons were not well-stained with antibody to SV2, despite often lying adjacent to neurons with extensive and bright im-

munostained calyces. We don't know whether this nonuniformity has a technical or a biological explanation. It is possible that some neurons have relatively few boutons on their surface and therefore appear unstained. Alternatively, the SV2 staining may simply not "work" on some cells. We think it unlikely that the SV2 staining is capricious at the level of individual boutons; if so, we would expect to find that bouton staining varies in intensity on individual cells, such that some were barely detectable while others were brightly stained. Instead, we find many well-stained boutons on most cells and none on others.

The spatial distribution of α-Bgt-AChR-containing patches on the neuronal surface was analyzed by examining the frequency with which 0, 1, 2, etc. patches were found within contiguous 5 or 10 μm lengths of the cell perimeter in optical sections, such as those shown in Figure 4*D–F* (Sargent and Pang, 1988). Patches were assumed not to occupy any space on the cell surface, so as not to reduce artificially the probability of finding several patches in a length. Individual experiments were made on four to eight optical sections from each of four neurons analyzed from a single experiment. Only every second or third optical section was used from reconstructions, to avoid multiple counting of individual patches. The mean number of patches per unit length was employed to generate an expected frequency distribution, using the Poisson equation, if the patches were randomly distributed over the surface. The Yates-corrected χ^2 test was used to compare observed and expected distributions (Glantz, 1992), and deviation from the expected distribution was taken as indicative of a nonrandom spatial distribution. The direction of the deviation indicated whether the patches tend to be clustered or evenly spaced.

Our ability to distinguish *qualitatively* between different labeling procedures (e.g., the degree of overlap between mAb 35-AChRs and synaptic sites in experiments on frozen sections versus those on whole mounts) was assessed by having one author prepare a coded set of images of 10–12 cells taken from each of two labeling paradigms and having the other author attempt to identify which cells belonged to the same set (coding was done by assigning random numbers to images). The statistical significance of the outcome was calculated by reference to the equation relating the probability of drawing, without replacement, k balls of either color in a sample of n balls from an urn containing M balls, of which M_w are white and $(M - M_w)$ are red (Parzen, 1960). Thus,

$$P(k) = \frac{\binom{M_w}{k}\binom{M - M_w}{n - k}}{\binom{M}{n}},$$

where

$$\binom{M_w}{k} = \frac{M_w!}{k!(M_w - k)!}, \quad \text{etc.}$$

When $M = 24$, $M_w = 12$, and $n = 12$, $P(8) = 0.18$ (not significant), $P(9) = 0.03$, $P(10) = 0.003$, $P(11) = 0.0001$, and $P(12) = 0.0000001$. In this instance, two sets of 12 images are said to be different if a naive observer can place at least 9 of each set in each of two 12 member groups. The probability of such an event happening by chance is 0.03 if the test is one-sided (9 red and 3 white) and 0.06 if it is two-sided (9 of one color, 3 of the other). The use of this procedure to compare two labeling procedures as regards their ability to alter the amount of overlap between AChRs and synaptic sites is referred, in the Results, as the *qualitative test.*

An estimate of the extent of overlap between immunofluorescently stained AChRs and synaptic sites was made on optical sections from whole-mounted tissue. The Optimas image analysis program was used to set thresholds for detection and define the borders of immunostained AChR clusters and synaptic sites, and the extent of overlap between the two was measured. The calculated values for overlap are useful for the purpose of comparison but are unlikely to have any absolute significance, since they are highly dependent on the values set for the threshold. The comparison between two incubation methods as regards their ability to alter the degree of overlap between AChRs and synaptic sites is referred, in the Results, as the *quantitative test.*

Sample means are given ± standard deviation (SD). Samples were compared using the Student's t test, or, when normality tests failed, the Mann-Whitney test.

Results

Virtually all ciliary ganglion neurons in chicken embryos have both mAb 35-AChRs and α-Bgt-AChRs

MAb 35 and mAb 210, which recognize similar or identical epitopes in *Torpedo* AChR (Saedi et al., 1990) and which also recognize the chick neuronal α5 subunit (Conroy et al., 1992), stain both the surface and the interior of neurons in frozen sections of embryonic ciliary ganglia (Fig. 1*A,B*). The intracellular immunoreactivity is absent from the nucleus (e.g., see neurons marked with asterisks in first panel of Fig. 1*A*), and within the cytosol it is present as bright spots that may represent elements of the rough endoplasmic reticulum and Golgi apparatus, where mAb 35 is known to bind on the basis of an electron microscopic analysis (Jacob et al., 1986). We assume that any signal represents clusters of AChRs rather than individual molecules.

We made a quantitative analysis of immunofluorescence within the interior of neurons by comparing the intensity of mAb 35 or mAb 210 staining with that of control mAb 12. MAb 12 is a rat anti-electric organ AChR that does not cross-react with chicken muscle AChRs (Tzartos and Lindstrom, 1980) or, apparently, chicken neuronal AChRs. The average gray value (pixel intensity) of rectangular fields from the interior of neurons stained with mAb 35 or mAb 210 was significantly greater than for neurons stained with mAb 12 or for neurons not incubated with primary antibody ($p < 0.001$ for each comparison, Fig. 2). To determine the proportion of ciliary ganglion neurons that express AChRs, we used an image analysis program to define AChR immunoreactivity as occurring wherever the average gray value over any part of the neuron exceeded a defined threshold, which was set after examining tissue incubated under control conditions (see Materials and Methods). The results of this analysis demonstrate that virtually all neurons in the ganglion have mAb 35-AChRs (Table 1).

A large majority of neurons in frozen sections showed surface staining and/or intracellular staining with Cy3-α-Bgt (Fig. 1*D*). The intracellular staining, like that seen with mAb 35 and mAb 210, was found only in the cytosol and consisted of brightly labeled spots. Both surface and intracellular staining were blocked completely by preincubating and coincubating tissue with a 100-fold molar excess of unconjugated α-Bgt (Fig. 1*E*). Quantitative analysis of intracellular staining indicated that the average gray value of rectangular fields from the interior of neu-

→

Figure 1. Anti-AChR ligands mAb 35, mAb 210, and α-Bgt specifically bind to embryonic ciliary ganglion neurons in frozen sections. Each panel depicts a field of neurons imaged using a confocal microscope from the interior of a 12 μm frozen section stained with the ligand indicated. Neurons in *A, B,* and *C* were taken from sections incubated with a mAb followed by a Cy3-goat anti-rat IgG. Neurons in *D* and *E* were stained with Cy3-α-Bgt, with or without excess, unlabeled α-Bgt. Specific staining is absent from the nuclei (see cells marked with *asterisks* in *A, left panel*). All images were collected using the same photomultiplier gain, and thus mAb 35 and mAb 210 staining, which benefit from the amplification through the use of secondary antibodies with high dye/protein ratios, is brighter than α-Bgt staining. MAb 210 staining is typically brighter than mAb 35 staining in fixed tissue, although both mAbs are thought to recognize the same antigen. Scale bar in *E, right panel,* applies to all images and represents 30 μm.

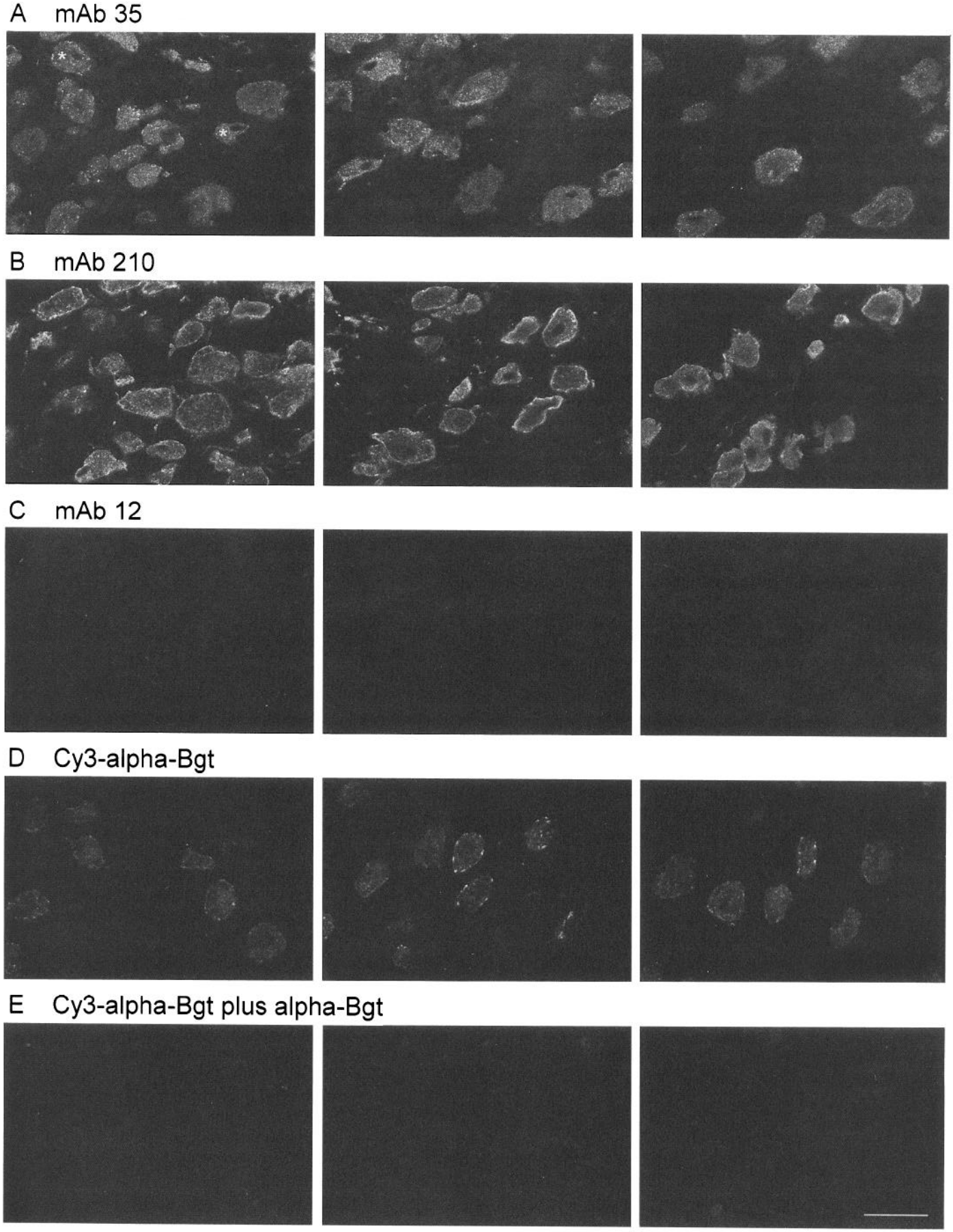
A mAb 35
B mAb 210
C mAb 12
D Cy3-alpha-Bgt
E Cy3-alpha-Bgt plus alpha-Bgt

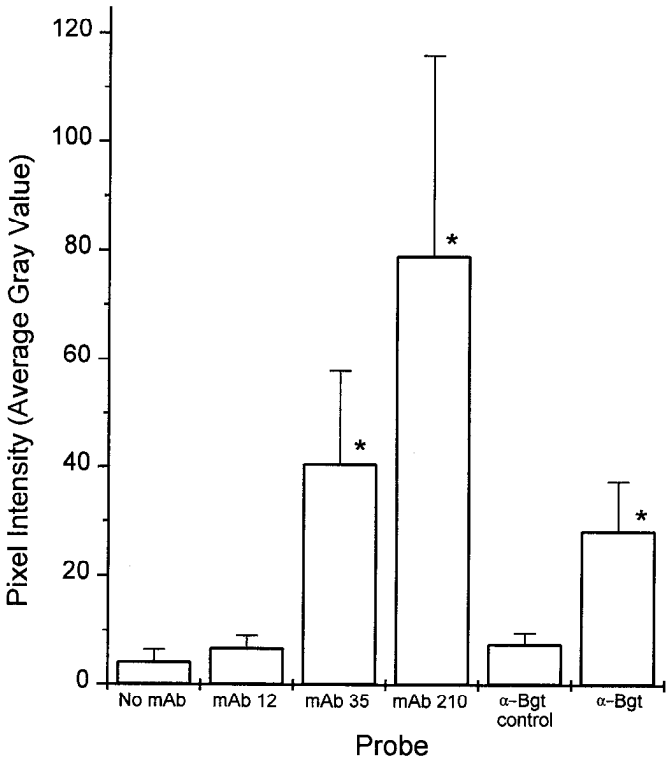

Figure 2. Fluorescence intensity arising from embryonic ciliary ganglion neurons is significantly greater when stained with mAb 35, mAb 210, or α-Bgt than under control conditions. The intensity of fluorescence signal arising from the interior of neurons such as those imaged in Figure 1 was measured from all neurons in 10 randomly selected fields and displayed as the mean ± SD. The number of neurons analyzed in the 10 fields ranged from 72 to 128 across the five experimental conditions and was not significantly correlated with average pixel intensity. *Asterisk* indicates $p < 0.001$ for comparison with appropriate control. Similar results were obtained in a second analysis.

rons incubated with Cy3-α-Bgt was significantly greater than that of cells taken from "control" sections treated with both Cy3-α-Bgt and excess, unlabeled α-Bgt ($p < 0.001$ by Mann-Whitney test, Fig. 2). To learn what proportion of neurons have α-Bgt-AChRs, we again used an image analysis program to define AChRs based on their gray value as compared to controls. As was true for mAb 35-AChRs, we found that virtually all neurons in the ciliary ganglion express α-Bgt-AChRs (Table 1).

Visualization of the preganglionic calyx in late embryonic neurons

Ciliary neurons are innervated by about 7 d of development. By 14 d, the dendrites elaborated by these cells have retracted, and a single preganglionic axon has expanded its terminal to cover a sizable fraction of the target cell, forming a calyx (Landmesser and Pilar, 1972). In anticipation of attempts to examine the location of mAb 35-AChRs and of α-Bgt-AChRs in relation to this calyx, we imaged calyces of embryonic ciliary neurons in whole-mounted ganglia with a laser scanning confocal microscope, using mAb 10h, which recognizes the SV2 glycoprotein (Buckley and Kelly, 1985). Figure 3 shows several views of immunocytochemically visualized calyces, both in optical sections through the middle (*A*) and upper surface (*B*) of neurons, as well as in stereopairs (*C,D*). The calyx clearly covers a substantial fraction of the neuronal surface. There is much variability in the appearance of the calyx from cell to cell, as judged by the pattern of SV2 immunoreactivity. In some instances, the antigen is mottled (e.g., Fig. 3*C*), while in others it consists of a large number of discrete regions (Fig. 3*D*). Interruptions in the SV2 staining are likely to represent areas within the calyx having few or no synaptic vesicles, rather than areas lacking the preganglionic terminal altogether, inasmuch as the calyx is thought to cover, without interruption, large expanses of the ganglion cell surface (Hess, 1965). Reference will be made to these nonsynaptic, contact regions (Loring and Zigmond, 1987) later in the Results section.

Table 1. Proportion of embryonic ciliary ganglion neurons expressing AChRs

AChR class	Percentage of neurons expressing AChRs (number of neurons) Experiment 1	Experiment 2
mAb 35-AChRs		
mAb 35	100% (95)	97% (87)
mAb 210	100% (128)	100% (73)
mAb 12 (control)	1% (72)	0% (71)
α-Bgt-AChRs		
Cy3-α-Bgt	88% (75)	99% (112)
Cy3-α-Bgt plus α-Bgt (control)	0% (83)	0% (106)

Relationship between α-Bgt-AChRs and synaptic sites on embryonic neurons

We examined the distribution of α-Bgt-AChRs in embryonic ciliary ganglion neurons by incubating fixed, unpermeabilized whole-mounts of ganglia with Cy3-α-Bgt. Optical sections taken through the middle of ciliary ganglion neurons stained with Cy3-α-Bgt reveal extensive and nonuniform surface staining, as well as a number of intracellular granules (Fig. 4*A*). Intracellular staining may result because fixation permeabilizes the neuronal membrane to Cy3-α-Bgt. Some of the surface staining appears to project as much as 1–2 μm from the surface (Fig. 4*A1,A3,* arrows). No staining is detected when incubations included a 100-fold molar excess of unlabeled α-Bgt (not shown; see frozen section controls, Fig. 1*E*). We assume that the surface staining represents α-Bgt-AChRs in the plasma membrane, both because of its appearance in optical sections and because intracellular staining, when evident, is clearly distinct from surface staining. We assume, further, that the surface staining identifies α-Bgt-AChRs principally on postganglionic neurons, since ciliary ganglion neurons retain α-Bgt-AChRs after denervation (Jacob and Berg, 1987) and since they make α-Bgt-AChRs when cultured in the absence of preganglionic neurons (Smith et al., 1983). We cannot rule out the possibility, however, that some α-Bgt-AChRs visualized here are presynaptic and situated on the synaptic surface of preganglionic terminals.

The nature of the surface staining obtained with Cy3-α-Bgt is best revealed when optical sections are taken through the upper surface of the neuron, as illustrated in Figure 4*B,* or when entire neurons are reconstructed and illustrated as stereo pairs (Figs. 4*C–F*). The most obvious staining (Fig. 4*C,F*) occurs in ovoid-shaped "blobs" or patches, measuring 2.7 ± 0.8 (long axis) by 1.6 ± 0.4 μm (short axis, $n = 36$ patches on eight neurons). Figure 4*C* shows a stereopair of a reconstructed cell with about 30 patches of α-Bgt-AChRs on its surface. About

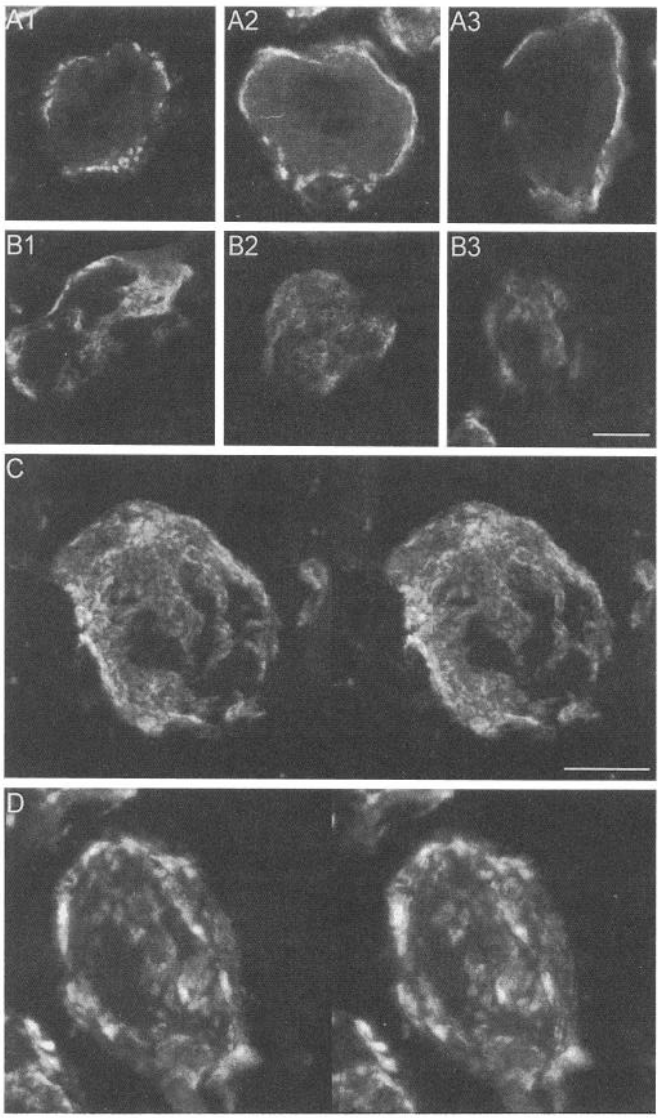

Figure 3. Some neurons in the embryonic ciliary ganglion are densely supplied by preganglionic terminals bearing synaptic vesicle antigen. All images are of embryonic ciliary ganglion neurons stained with anti-SV2 mAb 10h followed by Cy5-goat anti-mouse IgG. *A1, A2,* and *A3* show examples of optical sections taken through the middle of individual neurons. *B1, B2,* and *B3* show "glancing" sections taken through the upper surface of individual neurons (different from those depicted in *A1, A2,* and *A3*). *C* and *D* show stereopair views of stained neurons. A significant fraction of the surface of these cells is immunoreactive for SV2. In some instances the immunoreactivity is mottled (*C*), while in others it is fragmented into many discrete elements (*D*). Scale bar in *B3* (for *A* and *B*), 10 μm. Scale bar in *C* (for *C* and *D*), 10 μm.

60% of embryonic neurons (41 of 66 neurons sampled) incorporated nearly all of their detectable α-Bgt-AChRs into well-defined blobs, with the mean number per neuron, determined by eye, being 26 (SD = 8). The blobs do not appear to be uniformly fluorescent and may consist of a dense array of small, AChR clusters (Fig. 4*B,* insets). Other cells, such as the one illustrated in the stereopair in Figure 4*D,* have patches of α-Bgt-AChRs with less well-defined edges than those seen in Figure 4, *C* or *F*: these cells, having "wispy" patches of α-Bgt-AChRs, comprise about 30% of the population. Finally, a few neurons had many smaller, punctate AChR clusters (Fig. 4*E*). Clearly, there is a substantial degree of heterogeneity in the distribution of α-Bgt-AChRs on the neuronal surface, but in all instances, α-Bgt-AChRs were distributed nonuniformly and widely over the neuronal surface.

α-Bgt-AChR-containing patches on many cells appear to be evenly spaced over the neuronal surface (Fig. 4*C,F*). To analyze the surface distribution of α-Bgt-AChR patches, we measured the incidence with which 0, 1, 2, etc. patches were found in constant-sized bins in optical sections, and we compared the observed distribution with that expected if the patches were distributed randomly, that is, if they tended neither to cluster nor to be evenly spaced (generated from the Poisson equation). In each of three comparisons (Table 2) we found a significant deviation between observed and expected distributions. The deviation was in the direction of even spacing: that is, we observed more "1's" than expected and correspondingly fewer "0's" and "≥2's."

A spatial comparison between α-Bgt-AChRs and synaptic sites, detected immunocytochemically using anti-SV2, reveals that the patches of α-Bgt-AChRs are almost exclusively extrasynaptic (Fig. 6*A–C*). Figure 6*A* shows an optical section from the upper surface of a neuron stained both for α-Bgt-AChRs (left panel, blue) and synaptic sites (middle panel, red). Two prominent α-Bgt-AChR patches are nearly surrounded by areas of SV2 immunoreactivity. The merged image (Fig. 6*A,* right panel, see also inset) shows almost no evidence of colocalization (magenta). Many of the patches of α-Bgt-AChRs lie within gaps or interruptions in the regions of SV2 immunoreactivity, as illustrated in three additional examples shown in Figure 6*B.* Occasionally, we did find subtle examples of overlap between areas of α-Bgt-AChR immunoreactivity and synaptic sites, but these occurred at a frequency of fewer than one instance per 10 merged images, even when we used more favorable colors, such as green and red, to mark the location of α-Bgt-AChRs and synaptic sites, and even when we examined merged images on the computer screen, where they are more vibrant than in prints. The dominant observation, rather, is that the α-Bgt-AChR-rich areas are surrounded partly or completely by synaptic vesicle-rich sites but are themselves free of synaptic antigens. The patches containing α-Bgt-AChRs are rarely found over parts of the cell surface that lie some distance from the calyx (see Fig. 6*B1*). Thus the α-Bgt-AChRs are not simply extrasynaptic; more accurately, they are perisynaptic. Figure 6*C* shows a stereopair stained for both α-Bgt-AChRs and synaptic sites. Again, surface patches containing α-Bgt-AChRs are perisynaptic. The magenta color at the edges of the cell does not reliably indicate overlap, since the resolution of the technique is not sufficient in the z-axis to rule out a perisynaptic location.

The failure of Cy3-α-Bgt (MW 8700) to stain synaptic sites cannot readily be explained by the failure of the reagent to gain access to these sites. Unconjugated neuronal bungarotoxin (κ-Bgt), which is larger than α-Bgt, has access to synaptic sites in living, intact ganglia in minutes (Chiappinelli, 1983), and we would expect that a peptide having a relative molecular mass of less than 10 kDa would have access to the synaptic cleft in fixed, desheathed, halved ganglia during the 3 hr incubation used here.

Relationship between mAb 35-AChRs and synaptic sites in embryonic neurons

We examined the distribution of mAb 35-AChRs in embryonic ciliary ganglion neurons by incubating fixed, unpermeabilized whole-mounts of ganglia with mAb 35 or mAb 210, which appear to have a similar specificity both in *Torpedo* (Saedi et al.,

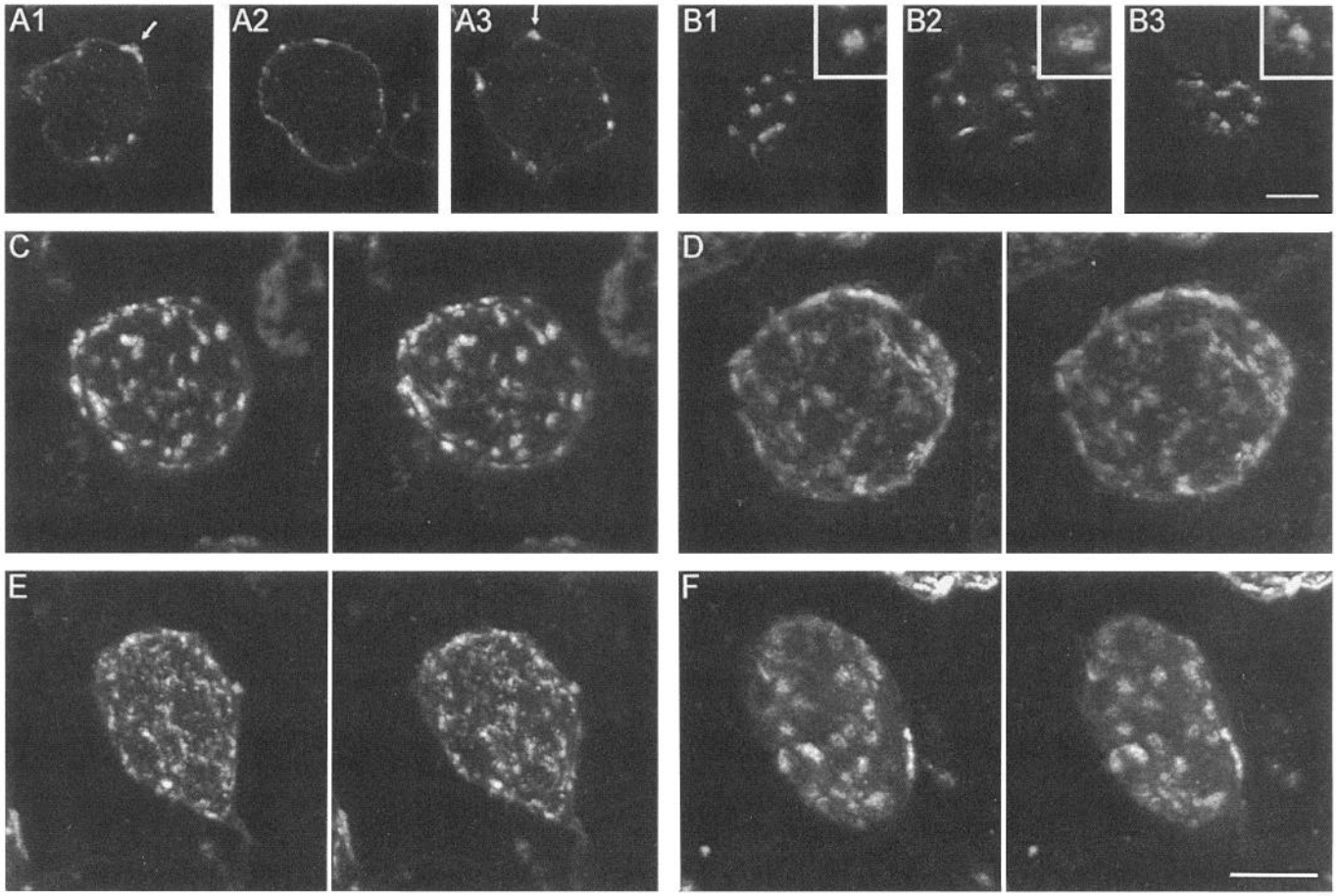

Figure 4. α-Bgt-AChRs are distributed widely over the surface of embryonic ciliary ganglion neurons. All images were obtained with the confocal microscope from neurons incubated with Cy3-α-Bgt in whole mounts, as described in Materials and Methods. *A* shows three examples of optical sections taken through the middle of individual ganglion neurons. Most of the binding is to the neuronal surface, although some intracellular staining is apparent. Surface staining is present around the entire cell surface but is most prominent in "blobs," which in some instances protrude slightly from the cell surface (*arrows* in *A1* and *A3*). On an "en face" view, provided by imaging optical sections from the upper surface of the neuron (*B*), the blobs are round or oval in shape and are nonuniform in staining intensity, presumably because they consist of numerous, small clusters of α-Bgt-AChRs (*inset*). Stereopairs (*C–F*) show that α-Bgt-AChRs are found over much of the cell surface. Most of the α-Bgt-AChRs appear to be in blobs, which typically number 20–30 per cell. Some neurons display α-Bgt-AChRs in clusters that are smaller and more numerous, such as that illustrated in *E*. Scale bar in *B3* (for *A* and *B*), 10 μm. Scale bar in *F* (for *C–F*), 10 μm.

1990) and the chicken ciliary ganglion (Conroy et al., 1992). Preincubation of whole ganglia with mAb 35 or mAb 210 completely blocked subsequent binding of Cy3-mAb 35 (not shown), and we therefore have used mAbs 35 and 210 interchangeably to identify mAb 35-AChRs. MAbs 35 and 210 bind to surface AChRs in intact, living ciliary ganglia (not shown, see Jacob et al., 1984), and thus presumably recognize an extracellular epitope.

MAb 35-AChRs, like α-Bgt-AChRs, were distributed nonuniformly and widely over the surface of embryonic ciliary ganglion neurons in whole mounts, as illustrated in optical sections through the middle of neurons (Fig. 5*A*). Internal staining, visible in some optical sections through the middle of the cell (e.g., Fig. 5*A3*) is not likely to represent internalization of antibody-labeled surface AChRs, since incubations were carried out on fixed tissue. Rather, the fixation procedure alone may produce a limited degree of permeabilization of the neuron's plasma membrane. Much of the surface mAb 35-AChR staining is concentrated in patches which, like α-Bgt-AChR-containing patches, often appear to project from the cell body by 1–2 μm (Fig. 5*A1* and 5*A2*, arrows). We assume that the surface staining represents mAb 35-AChRs in the plasma membrane, both because of its appearance in optical sections and because intracellular staining, when evident, is clearly distinct from surface staining. We assume further that the surface binding identifies mAb 35-AChRs principally on postganglionic neurons, since mAb 35-AChRs identified at the neuronal surface by electron microscopic immunoperoxidase techniques are retained following denervation (Jacob and Berg, 1988). We cannot rule out the possibility, however, that some of the mAb 35-AChRs visualized here are pre-

Table 2. Distribution of α-Bgt-AChR-containing patches on the surface of embryonic neurons

Exp.	Observed			Expected				
#	0	1	≥2	0	1	≥2	χ^2	*P*
1	70	58	10	77.9	44.6	15.5	6.05	<0.01
2	97	76	16	106.1	61.2	21.6	5.24	<0.01
3	109	96	21	122.7	74.9	28.4	8.77	<0.005

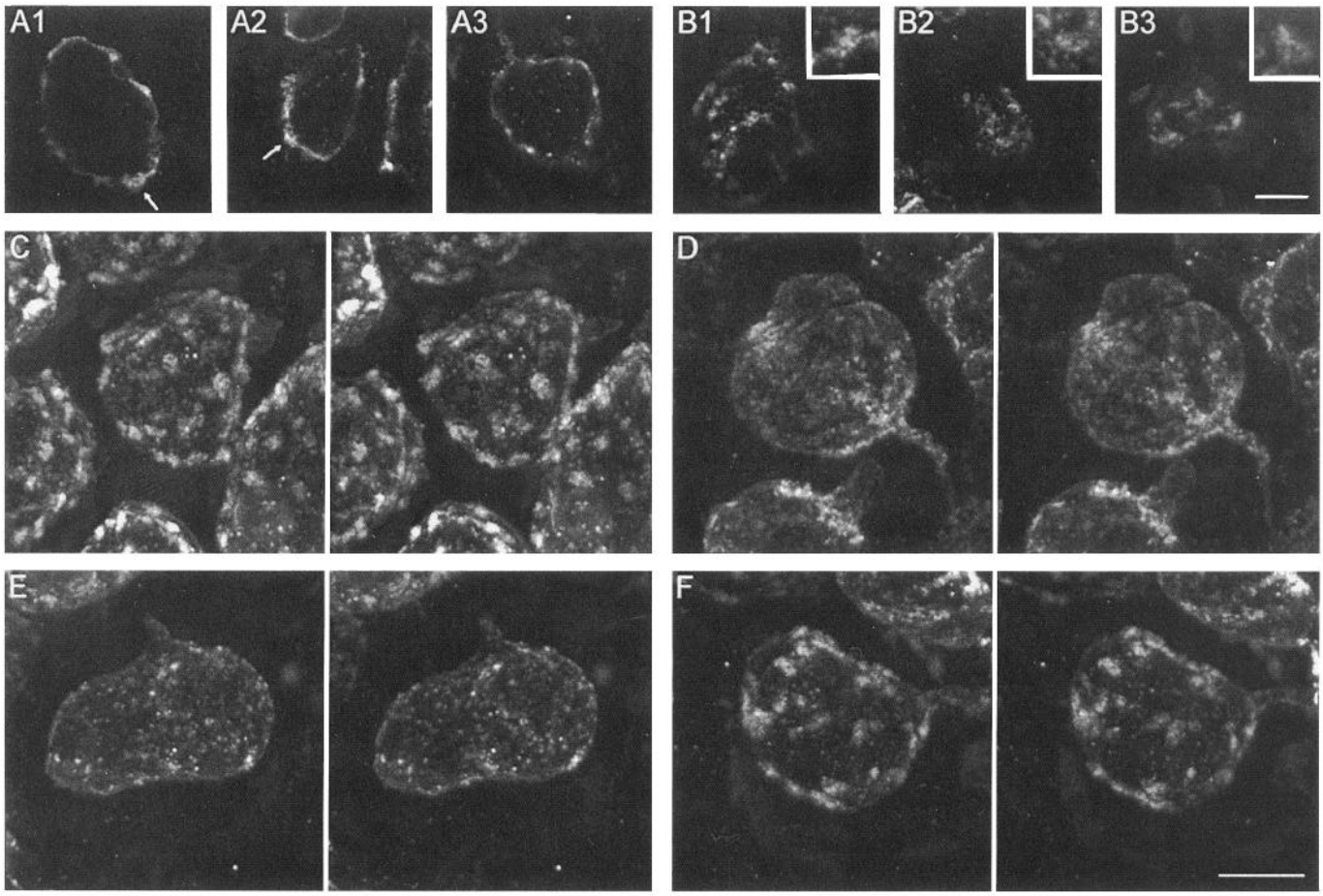

Figure 5. mAb 35-AChRs are distributed widely over the surface of embryonic ciliary ganglion neurons. All images were obtained with the confocal microscope from neurons incubated with Cy3-mAb 35, or with mAb 210 and Cy3-goat anti-rat IgG. *A* shows three examples of optical sections taken through the middle of individual ganglion neurons. Most of the signal arises from the neuronal surface, although some intracellular staining is present (see *A3*). Much of the surface signal is concentrated in "blobs," which in some instances protrude slightly from the cell surface (*arrows* in *A1* and *A2*). On an "en face" view, provided by imaging the upper surface of the neuron (*B*), the blobs resemble, both in size and shape, those displaying α-Bgt-AChRs (*insets*). Additionally, however, mAb 35-AChRs are present in punctate clusters, some of which are visible in *B1* and *B2*. Stereopairs (*C–F*) show that mAb 35-AChRs, like α-Bgt-AChRs, are found over much of the cell surface. On many cells (e.g., *C* and *F*) the blobs are the principal source of mAb 35-AChRs on the neuronal surface. Some neurons display other patterns of mAb 35-AChRs, where the blobs are smaller (*E*) or where they are less well-defined (*D*). Scale bar in *B3* (for *A* and *B*), 10 μm. Scale bar in *F* (for *C–F*), 10 μm.

synaptic and confined to the synaptic surface of preganglionic terminals.

When viewed in "glancing" optical sections through the upper surface of the neuron, mAb 35-AChR-containing patches are similar in size to α-Bgt-AChR-containing patches and nonuniform in staining intensity. Patches of mAb 35-AChR clusters, like patches of α-Bgt-AChRs, ranged from "blobby" to "wispy." A notable difference between the distribution of α-Bgt-AChRs and of mAb 35-AChRs was that many neurons had numerous, small, punctate clusters of mAb 35-AChRs (e.g., Fig. 5*B,C*). While more than half of the reconstructed neurons showed a combination of well-defined blob-like staining, with punctate, spot-like staining, as illustrated in Figure 5, *C* and *F,* other cells had clusters of mAb 35-AChRs that were intermediate in appearance (Fig. 5*D,E*).

Double label experiments, in which both mAb 35-AChRs and synaptic sites are marked with different fluorophores, show that the patch-like areas containing mAb 35-AChRs are exclusively extrasynaptic, as noted previously for patch-like areas containing α-Bgt-AChRs. The relationship between the small, punctate areas of mAb 35-AChRs and synaptic sites was often more subtle, as is illustrated in Figure 6*D–F*. Figure 6*D* shows the distribution of mAb 35-AChRs, colored green, and synaptic sites, colored red, in an optical section from the upper surface of a neuron. MAb 35-AChRs are present in several blobs and in a constellation of small, punctate clusters in the upper left quadrant of the cell (left panel). This region is also immunoreactive for SV2 (middle panel), thus leading to the expectation that there will be extensive colocalization between small AChR clusters and synaptic sites. Indeed, a color merge (right panel) shows some overlap, in yellow, between mAb 35-AChRs and synaptic sites (clearest in inset). However, despite the fact that a large degree of *course* overlap exists between the location of mAb 35-AChR clusters and synaptic sites over a sizable region of the cell, the two antigens are rarely in perfect register. Additional examples of color merges from glancing, surface sections taken from individual neurons are illustrated in Figure 6*E*. In Figure 6*E1* (inset), several clusters of mAb 35-AChRs, rendered green, lie adjacent to and between areas of SV2 immunoreactivity. In some instances, clusters of mAb 35-AChRs are colocalized at synaptic sites, as marked by the presence of yellow dots (see Fig. 6*E1,* inset, arrow). In many instances regions of overlap lie

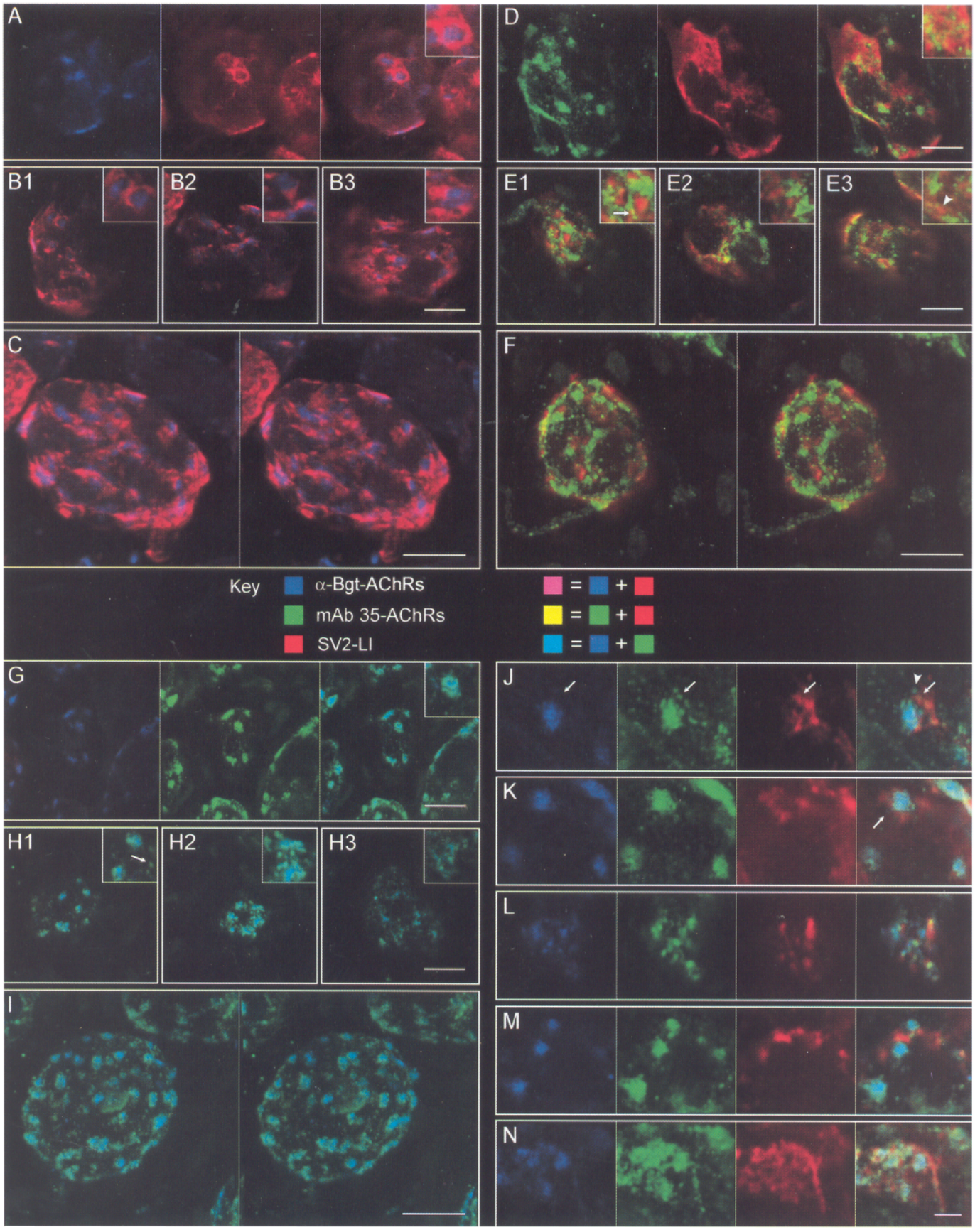
A
B1
B2
B3
C
D
E1
E2
E3
F
Key
α-Bgt-AChRs
mAb 35-AChRs
SV2-LI
= +
= +
= +
G
H1
H2
H3
I
J
K
L
M
N

at the margin of synaptic immunoreactivity, rather than at their centers (Fig. 6*D*, right, inset). Most of the small mAb 35-AChR clusters are extrasynaptic, however, as demonstrated by a preponderance of green, as opposed to yellow, color in merged optical sections or in merged stereopairs (Fig. 6*F*). Another form of overlap between mAb 35-AChRs and synaptic sites, which is more difficult to detect, is the presence of low to moderate levels of mAb 35-AChR signal extending over larger areas and overlapping with synaptic sites (e.g., Fig. 6*E3*, inset, arrowhead). Some synaptic sites appear not to have mAb 35-AChRs, and overall, only a small fraction of the detectable mAb 35-AChRs are synaptic.

Relationship between mAb 35-AChRs and α-Bgt-AChRs on embryonic neurons

Since both mAb 35-AChRs and α-Bgt-AChRs are found in patch-like areas on the neuronal surface, it is natural to ask whether common regions of the surface express both AChR classes. Double label experiments demonstrate that they, in fact, do. Figure 6*G* shows optical sections of the upper surface of a neuron stained for α-Bgt-AChRs (left panel, blue) and mAb 35-AChRs (middle panel, green). The merged image (Fig. 6*G*, right panel) shows colocalization of mAb 35-AChRs and α-Bgt-AChRs (cyan) in a patch measuring about 2 × 3 μm. Careful examination of merged images indicates that the patches containing both AChR classes are not uniformly colored; rather, they often appear variegated. This suggests that the two AChR classes within them are not precisely colocalized. In Figure 6*G*, inset, spot-like clusters of both α-Bgt-AChRs (blue) and mAb 35-AChRs (green) are evident in areas adjacent to the patch containing both AChR classes (cyan). Figure 6*H* shows three additional examples of merged images; in each instance the neuronal surface has patch-like regions containing both AChR classes. Smaller, punctate clusters containing only mAb 35-AChRs are quite common in regions adjacent to these patches (Fig. 6*H1*, inset, arrow), but clusters containing only α-Bgt-AChRs are rare. Most areas displaying patch-like immunoreactivity for one AChR class also show it for the other; for example, the neuron depicted in the stereopair (Fig. 6*I*) has 30–40 patches on its surface, every one of which has some blue and some green color.

We performed triple label experiments to examine the relative location of α- Bgt-AChRs (blue), mAb 35-AChRs (green), and synaptic sites (red). Figure 6*J–N* illustrate the outcome of imaging the upper surface of five different neurons from a triple-labeled ciliary ganglion. In the merged images (right panels), the α-Bgt-AChR- and mAb 35-AChR-containing patches are cyan, while areas of overlap between mAb 35-AChRs and synaptic sites are yellow. Areas where all three colors colocalize appear light or white. Some of the punctate mAb 35-AChR-only clusters are synaptic. Figure 6*J* shows an area, containing mAb 35-AChRs but lacking α-Bgt-AChRs, that is located at a synaptic site (arrows). Two adjacent mAb 35-AChR clusters are also synaptic, while a third is located about 0.5 μm from a synaptic site (arrowhead in right panel). Figure 6*K* shows several small, mAb 35-AChR-containing clusters adjacent to a larger patch containing both α-Bgt-AChRs and mAb 35-AChRs; here, as in Figure 6*J*, the patch is partly surrounded by SV2 immunoreactivity, but in this example most of the clusters are extrasynaptic (arrow). Figure 6*L* and *M* illustrate other instances where some, but not all, punctate regions containing only mAb 35-AChRs are synaptic and appear yellow in the merged images (right panels). Figure 6*N* illustrates a more complicated example where a larger area containing many AChR clusters is also occupied by a region of the preganglionic arbor stained for SV2 antigen; the merged image shows some extrasynaptic patches containing both AChR classes (cyan) as well as a few regions, adjacent to

←

Figure 6. Comparison of the distribution of α- Bgt-AChRs, mAb 35-AChRs, and SV2 immunoreactivity in embryonic ciliary ganglion neurons. Each molecule is consistently rendered a different color, according to the key (*center*). Colocalization of two molecules will be revealed by magenta (blue plus red), yellow (green plus red), or cyan (blue plus green), as indicated in the key. The first three quadrants (*A–C, D–F,* and *G–I*) display the results of pair-wise comparisons, while the last quadrant (*J–N*) displays the results of triple label experiments. *A–C* show the relative location of α-Bgt-AChRs (blue) and synaptic sites (SV2 immunoreactivity, red). *A* shows the distribution of α-Bgt-AChRs in the *left panel,* of synaptic sites in the *middle panel,* and of both in the *right panel,* all for an optical section that grazes the upper surface of a ciliary ganglion neuron. The *right panel* in *A,* and its *inset,* shows that patch-like regions containing α-Bgt-AChRs are adjacent to, and often surrounded by, synaptic sites. Areas of apparent overlap near the edge of the cell (bottom of cell in *A, right panel*) are not necessarily due to true overlap, since the spatial resolution of the confocal microscope in the z direction is less than in the x or y directions. Similar results are shown in *B,* which shows three additional examples of merges (as in *A, right panel*). *C* shows a stereopair that demonstrates the perisynaptic nature of the patches of α-Bgt-AChRs. *D–F* show the relative location of mAb 35-AChRs (green) and synaptic sites (SV2 immunoreactivity, red). *D* shows the distribution of mAb 35-AChRs in the *left panel,* of synaptic sites in the *middle panel,* and of both in the *right panel,* all for an optical section that grazes the upper surface of a ciliary ganglion neuron. The *right panel in D,* and its inset, shows that some overlap exists between surface regions rich in mAb 35-AChRs and those rich in synaptic vesicles. While the larger, patch-like areas containing mAb 35-AChRs tend to be extrasynaptic, there are arrays of smaller, punctate clusters of mAb 35-AChRs, some of which overlap with synaptic sites, indicated by the presence of yellow spots in the merged image (and *inset*) and in additional examples (*E1, arrow*). The *arrowhead* in the *inset* of *E3* indicates a second type of overlap characterized by diffuse areas of mAb 35-AChR immunoreactivity that are centered at synaptic sites. *F* shows a stereopair illustrating that most of the mAb 35-AChRs are extrasynaptic and are green, as opposed to yellow, in merged images. *G–I* show the relative location of α-Bgt-AChRs (blue) and mAb 35-AChRs (green). *G* shows the distribution of α-Bgt-AChRs in the *left panel,* of mAb 35-AChRs in the *middle panel,* and of both in the *right panel,* all for an optical section that grazes the upper surface of a ciliary ganglion neuron. The *right panel* in *G,* and its *inset,* shows that the patch-like regions containing α-Bgt-AChRs also contain mAb 35-AChRs and are rendered cyan in the color merge (see *inset*). The color of the patches in merged images is often not uniform, suggesting that the two AChRs are not exactly in register. Similar results are shown in *H,* which shows three additional examples of merges (as in *G, right panel*). Numerous green (mAb 35-AChRs) spots appear on the neuronal surface unaccompanied by detectable concentration of α-Bgt-AChRs (*H1, inset, arrow*). *I* shows a stereopair that demonstrates extensive overlap between α-Bgt-AChRs and mAb 35-AChRs. All patches on this cell containing α-Bgt-AChRs also contain mAb 35-AChRs, and vice versa. *J–N* show the results of triple label experiments and depict, at high magnification, regions of the surface of individual neurons, taken from optical sections that graze the neuronal surface. The first three panels show the distribution of α-Bgt-AChRs, mAb 35-AChRs, and synaptic sites in common fields, while the *right panel* shows a color merge of all three distributions. The bulk of the α-Bgt-AChRs and the mAb 35-AChRs are found together in large, extrasynaptic patches (cyan). Some of the smaller areas containing mAb 35-AChRs and found adjacent to the patches are synaptic (*J, arrows*). Other AChR clusters, containing mAb 35-AChRs only (*K, right panel, arrow*) or both mAb 35-AChRs and α-Bgt-AChRs (*J, right panel, arrowhead*) are extrasynaptic. All scale bars in *A–I* are 10 μm. Scale bars in *A, D,* and *G* are for all images in the relevant quadrants except the stereopairs, which have their own scale bar. *Insets* in *B, E,* and *H* are magnified two times and measure 6 μm by 6 μm. Scale bar in *N* is 3 μm and is for *J–N*.

these patches, containing both mAb 35-AChRs and SV2 immunoreactivity (yellow). These triple label images show that some of the small clusters of mAb 35-AChRs found outside patches, are indeed synaptic. However, the AChRs in these clusters constitute only a small fraction of the total complement of surface mAb 35-AChRs visualized in these experiments. A majority of the clustered mAb 35-AChRs are found in extrasynaptic patches along with α-Bgt-AChRs.

Most mAb 35-AChRs are extrasynaptic even when incubation protocols are altered to promote antibody access into the synaptic cleft

The degree to which mAb 35-AChRs were found in extrasynaptic areas came as a surprise, inasmuch as previous results, analyzed by electron microscopy after incubating unfixed tissue with mAb 35-HRP, suggested a predominantly synaptic location of mAb 35-AChRs (Jacob et al., 1984). One possibility is that our protocol did not stain all synaptic sites with the anti-SV2 antibody and thus identifies clusters of mAb 35-AChRs as extrasynaptic when they are, actually, synaptic. We regarded this possibility as remote, since it would require that the labeling procedure identify some synaptic sites on the neuronal surface of lightly fixed and Triton X-100–permeabilized tissue but not others that may lie within one or a few micrometers. In other tissue we have shown that immunocytochemical techniques can quantitatively label synaptic sites (Sargent, 1983). To examine whether, for technical reasons, the SV2 labeling procedure might not identify all synaptic boutons and might thereby underestimate the extent of overlap between mAb 35-AChRs and synaptic sites, we compared the overlap noted under normal conditions with that noted after an incubation protocol in which we attempted to enhance the intensity of stained synaptic sites by doubling all parameters related to the immunocytochemical visualization procedure. Thus, we permeabilized tissue with 0.6% Triton X-100 for 60 min rather than with 0.3% Triton X-100 for 30 min. Incubations with mAb 10h (anti-SV2) and Cy5-goat anti-mouse IgG incubations were done for 6 hr rather than three, and their concentrations were doubled. Using a qualitative test (see Materials and Methods), we were unable to distinguish the degree of overlap between mAb 35-AChRs and synaptic sites seen following the normal incubation protocol from the overlap seen following the "2×" protocol. Moreover, SV2 staining was no more intense in the 2× condition than in the normal condition when assessed by noting photomultiplier gains needed to produce saturation of signal at synaptic sites (gray level = 255, not shown). This suggests that synaptic sites are stained maximally using our indirect immunofluorescence procedure and that the failure to find substantial colocalization between clusters of mAb 35-AChRs and synaptic sites is not due to inadequate visualization of synaptic sites. We cannot rule out the possibility, however, than some release sites within the calyx lack SV2 and are immunonegative for mAb 10h. It is unlikely, however, that such heterogeneity could explain our results, since previous electron microscopic evidence suggests strongly that both mAb 35-AChRs and α-Bgt-AChRs are located in pseudodendrite-containing regions of the neuronal surface that lack synaptic specializations (Jacob and Berg, 1983; Jacob et al., 1984; Loring et al., 1985; Loring and Zigmond, 1987).

Another possible explanation for the unexpectedly prominent extrasynaptic location of mAb 35-AChR clusters is that mAb 35 or mAb 210 does not have complete access to all synaptic clefts in our experiments, where lightly fixed ganglia are desheathed, cut in half to promote access, and incubated with antibodies for 3 or more hours per step. This results in heavy labeling of nearly all neurons within the cortical 50–100 μm of the ganglion, and we typically examine only the superficial 25–50 μm of this layer. Nevertheless, it is still possible that mAbs 35/210 and fluorescent secondary IgGs do not completely penetrate into the synaptic cleft under these conditions. To test this hypothesis, we altered the incubation protocol in three ways designed to improve the degree of penetration of IgG-sized reagents into the synaptic cleft. In one procedure, we increased the duration of the incubation step with Cy3-mAb 35 from 3 hr to 24 hr, and in a second procedure we preincubated living ganglia with proteases to enhance access of large molecules to the synaptic cleft. In each instance, the procedure resulted in the labeling of neurons deep within the interior of the ganglion, suggesting that permeation of IgG-sized reagents had indeed been enhanced. In neither instance, however, did we find any more overlap between mAb 35-AChRs and synaptic sites in neurons located at the periphery of the ganglion, as revealed in either the qualitative test or the quantitative test (see Materials and Methods for details). Finally, in a third procedure we labeled both mAb 35-AChRs and synaptic sites in frozen sections rather than on whole mounts. The distribution of mAb 35-AChRs in these sections was largely extrasynaptic, as before, and in a qualitative test we again found no more overlap between mAb 35-AChRs and synaptic sites than occurred in a parallel experiment performed on whole mounts. Thus, there appears to be no additional colocalization between mAb 35-AChRs and synaptic sites when double label incubations are performed under conditions where one can expect markedly enhanced access of macromolecules to the synaptic cleft.

mAb 35-AChRs and α-Bgt-AChRs on neurons in adult ciliary ganglia

To examine the spatial relationship among mAb 35-AChRs, α-Bgt-AChRs, and synaptic sites in mature ganglia, we repeated the analysis on ganglia taken from 12–14 week chickens, which we will refer to as adults. Frozen section experiments, analogous to those illustrated in Figure 1, showed strong staining of neurons for both mAb 35 and mAb 210 and for α-Bgt (not shown). Quantitative measurements analogous to those illustrated in Figure 2 for embryonic neurons showed, as expected, that the staining with mAb 35, mAb 210, and α-Bgt is significantly brighter than neurons stained under control conditions (not shown). Finally, the use of thresholding and image analysis illustrates that in adults, as in embryos, virtually all neurons in the ciliary ganglion express both mAb 35-AChRs and α-Bgt-AChRs (Table 3).

Before describing the relationship between α-Bgt-AChRs or mAb 35-AChRs and synaptic sites, we examined the arrangement of synaptic vesicle antigen, and, by inference, of synaptic sites in adult ciliary ganglia. Unlike the situation in embryos, we found that relatively few adult neurons had calyceal endings on them (Hess, 1965). Rather, a typical neuron had numerous boutons on its surface. Figure 7 shows four examples, illustrated as stereopairs, of the arrangement of synaptic vesicle antigen on neurons in the adult ciliary ganglion. Only one of the four examples, Figure 7*C*, shows a pattern of immunoreactivity suggestive of a calyx. Occasionally, the SV2 pattern suggests that the calyx is retracting and giving rise to synaptic boutons (e.g., Fig. 9*F*). Adult neurons lacking a calyx typically have 30–60 round or oval boutons on their surface (Fig. 7*A,B,D*). The boutons vary in size, ranging from about 1 μm × 1 μm to as large

Table 3. Proportion of adult ciliary ganglion neurons expressing AChRs

AChR class	Percentage of neurons expressing AChRs (number of neurons) Experiment 1	Experiment 2
mAb 35-AChRs		
mAb 35	85% (55)	98% (47)
mAb 210	100% (36)	100% (53)
mAb 12 (control)	2% (51)	0% (50)
α-Bgt-AChRs		
Cy3-α-Bgt	100% (42)	100% (68)
Cy3-α-Bgt plus α-Bgt (control)	3% (38)	0% (50)

as 4 μm × 5 μm. Some of the boutons, especially the larger ones, sometimes occupied slight depressions in the neuron (apparent for some of the larger boutons in Fig. 7*B*).

The distribution of α-Bgt-AChRs on the surface of adult neurons was reminiscent of that noted in embryonic ganglia. As illustrated in Figure 8, *A* and *B*, which shows stereopairs of adult neurons labeled with Cy3-α-Bgt, most α-Bgt-AChR clusters are found in blobs or patches, which are distributed over the entire surface of the cell. The patches are round or ellipsoidal and are approximately the same size as in embryos, having an average dimensions of 2.6 ± 0.8 by 1.3 ± 0.4 μm (long and short axes; $n = 49$; long axis not different from long axis of patches measured on embryonic neurons, $P = 0.48$; short axis significantly different from embryonic mean of 1.6 ± 0.4 μm, $P = 0.004$). The number of patches per cell was larger in adult neurons, at 41 ± 22 ($n = 37$), than in embryonic neurons (26 ± 8, $P < 0.0001$ by Mann-Whitney test). There is some heterogeneity in the appearance of α-Bgt-AChR blobs; in Figure 8*B*, for example, they are less well-defined and more "wispy" than in Figure 8*A*. As was noted for embryonic ciliary ganglion neurons, most of the detectable α-Bgt-AChRs appear to be located in the blobs.

While α-Bgt-AChR-containing patches on adult neurons are widely distributed over the cell surface, a spatial analysis of their distribution revealed that they tended to be distributed randomly over the cell surface, in contrast to the situation in embryos. Thus, in two of three comparisons, the expected frequency of finding 0, 1, and ≥2, patches in 10 μm lengths of the cell surface in optical sections was not significantly different than that expected from the Poisson distribution, which assumes a random distribution (Table 4). Only in one of three instances (experiment #1) was there a significantly nonrandom distribution of patches, and in this instance the patches tended to be evenly spaced (too many observed "1's," too few observed "0's" and "≥2's"). Thus, while the tendency for α-Bgt-AChR-containing patches to be evenly spaced is strong on embryonic neurons, it is weak or nonexistent on adult neurons.

Simultaneous labeling of α-Bgt-AChRs and synaptic sites in 12–14 week chickens revealed a result somewhat similar to that obtained in embryos: namely, that most α-Bgt-AChRs are perisynaptic. Unlike the situation in embryos, however, patches or blobs containing α-Bgt-AChRs occasionally lie some distance from synaptic sites. Figure 9*A* shows the distribution of α-Bgt-AChRs (left panel, blue), SV2 immunoreactivity (middle panel, red), and a color merge of the left and middle panels (right panel). There is relatively little overlap between α-Bgt-AChRs

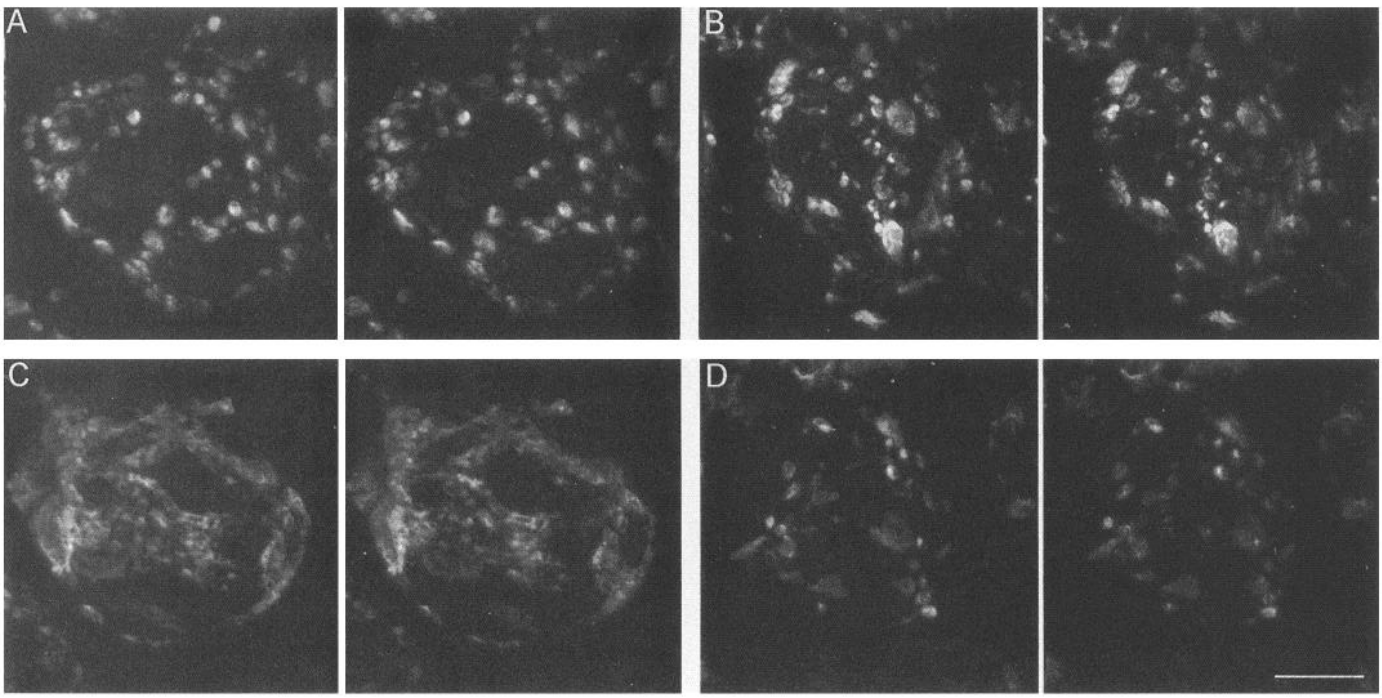

Figure 7. SV2 immunoreactivity on ciliary ganglion neurons from 12–14 week chickens. These four stereopairs (*A–D*) illustrate examples of the pattern of SV2 immunoreactivity (synaptic sites) on adult neurons. Synaptic calyces, such as that illustrated in *C*, were less common in 12–14 week chickens than in embryos. More commonly, neurons had many synaptic boutons of varying sizes on their surface. These boutons covered, collectively, a smaller proportion of the neuronal surface than densely innervated, bouton-containing terminals observed in embryos (compare to Fig. 3*D*).

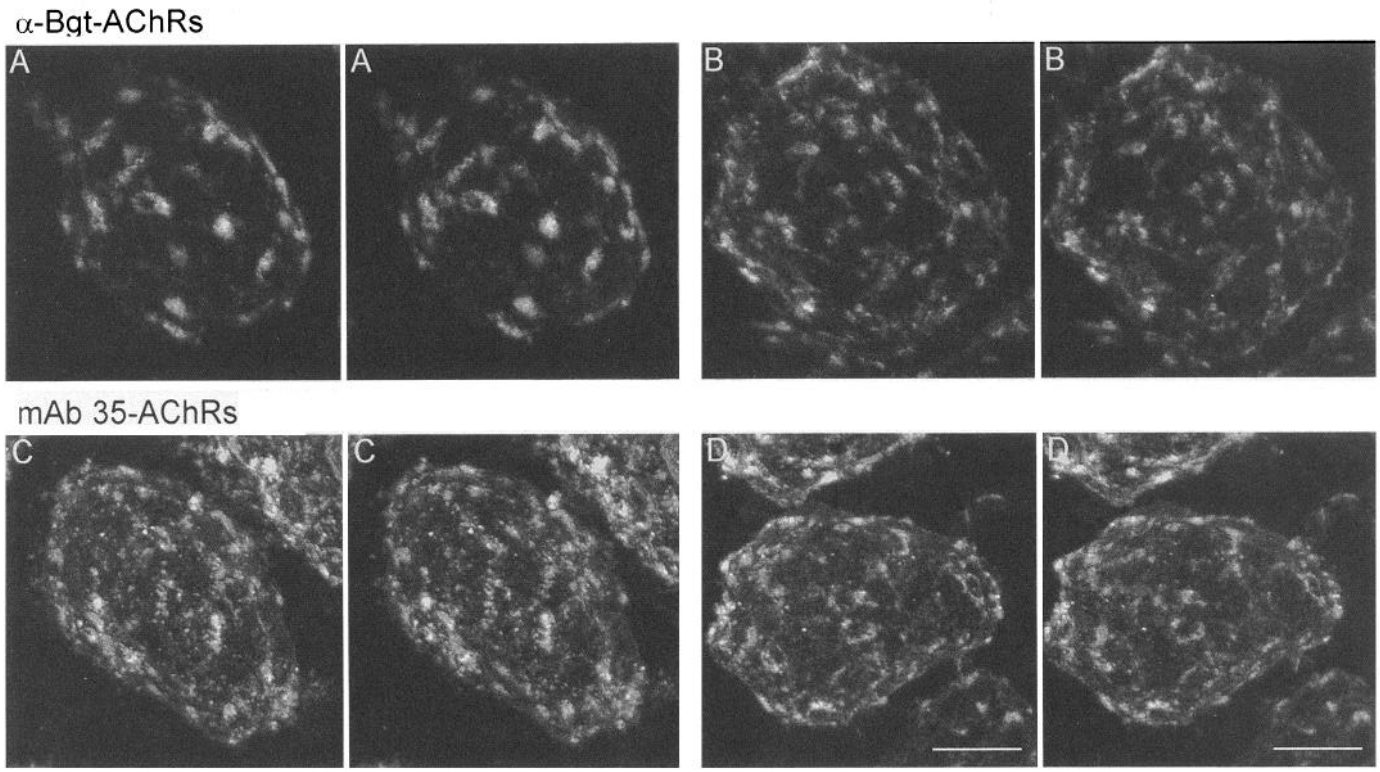

Figure 8. Distribution of α-Bgt-AChRs (*A, B*) mAb 35-AChRs (*C, D*) on the surface of adult ciliary ganglion neurons. α-Bgt-AChRs and mAb 35-AChRs are often arranged in blobs or patches with a widespread distribution on adult ciliary ganglion neurons, as in embryos (see Fig. 4). Scale bar (in *D*), 10 μm.

and synaptic sites. α-Bgt-AChRs tend to be found in patches, some of which occupy sites immediately adjacent to those containing synaptic vesicle antigen and some of which lie some distance from synaptic regions. Three additional examples are illustrated in Figure 9*B*. Bouton-like synaptic sites almost invariably lie adjacent to patches containing α-Bgt-AChRs (in 104 of 105 instances in one sample) and are often partially surrounded by such patches. This arrangement is just the reverse of that seen in embryonic neurons containing calyceal endings; there, the patches containing α-Bgt-AChRs are partially or completely surrounded by synaptic sites (compare Fig. 6*A–C* and Fig. 9*A–C*). What is seen consistently at the two stages is that most of the detectable α-Bgt-AChR clusters are perisynaptic. One subtle difference in the relationship between α-Bgt-AChRs and synaptic sites in embryonic and in adult neurons is that small clusters of α-Bgt-AChRs were occasionally found at the margin of synaptic boutons in adults. In embryos fewer than one in 10 merged images had examples of small α-Bgt-AChR-containing AChR clusters at synaptic sites, while in adults, perhaps half of the merged images examined contained examples (Fig. 9*B2*, inset).

Table 4. Distribution of α-Bgt-AChR-containing patches on the surface of adult neurons

Exp.	Observed			Expected				
no.	0	1	≥2	0	1	≥2	χ^2	*P*
1	68	61	14	74.6	46.3	22.1	7.46	<0.01
2	18	29	26	21.5	26.2	25.3	0.62	>0.25
3	39	45	26	43.5	40.4	26.1	0.81	>0.25

The distribution of mAb 35-AChRs on adult neurons is also somewhat similar to that noted for these AChRs on the surface of embryonic neurons. Figure 8, *C* and *D*, shows examples of two neurons illustrated as stereopairs. The neuron in Figure 8*C* is typical in having many patches or blobs of mAb 35-AChRs distributed widely over the surface of the neuron. Unlike the appearance of α-Bgt-AChRs in adults, however, most neurons also have numerous, smaller, punctate clusters of mAb 35-AChRs in addition to blobs, as found for embryonic neurons. As also noted for embryonic neurons, we found heterogeneity in the appearance of mAb 35-AChRs on the surface of adult neurons; in some instances the blobs were less pronounced or less well-defined (Fig. 8*D*). The relationship between mAb 35-AChRs and synaptic sites on adult neurons was examined by double label experiments and is illustrated in Figure 9*D–F*. Figure 9*D* shows an optical section taken through the upper surface of an adult ciliary ganglion neurons, showing mAb 35-AChRs in green (left panel) and synaptic sites in red (middle panel). The merged image (right panel; see also inset) shows that most regions of the neuronal surface that have detectable immunoreactivity for mAb 35-AChRs are extrasynaptic. The spatial relationship between the blobs of mAb 35-AChRs and synaptic sites in adult neurons is reminiscent of that between α-Bgt-AChR blobs and synaptic sites: the sites are rarely isolated but rather are typically adjacent to AChR-containing blobs. As illustrated in all three panels of Figures 9*E* and in the stereopair (Fig. 9*F*), patches of mAb 35-AChRs often lie immediately adjacent to synaptic boutons. There are, additionally, regions of

overlap between mAb 35-AChRs and synaptic boutons, which can occur when strongly stained, punctate clusters of mAb 35-AChRs are located at the border of synaptic boutons (e.g., Fig. 9*D*, right panel, inset, arrow), and when more diffuse regions having mAb 35-AChRs co-localize with synaptic boutons (e.g., Fig. 9*E3*, inset, arrowhead). These two forms of overlap were also found in embryos, and their incidence is not markedly different in the adult. Overall, however, most of the mAb 35-AChRs are extrasynaptic in adults, as in embryos.

Double label experiments in which we visualized both α-Bgt-AChRs and mAb 35-AChRs revealed the same general results as were noted in embryonic neurons. As illustrated in Figure 9*G–I*, virtually all membrane patches or blobs containing α-Bgt-AChRs also contain mAb 35-AChRs, and vice versa. While α-Bgt-AChRs tended to be restricted to these blobs, the mAb 35-AChRs were found, in addition, in smaller, punctate clusters over wide regions of the surface (Fig. 9*H2*, inset, arrow). As illustrated in triple label experiments (see below), some of these smaller clusters of mAb 35-AChRs are located at synaptic sites.

Figure 9*J–N* illustrates five fields from the surface of adult ciliary ganglion neurons imaged for α-Bgt-AChRs (blue), for mAb 35-AChRs (green), and for synaptic sites (SV2 immunoreactivity, red). The right panel of each image shows a color merge that illustrates the spatial relationship among α-Bgt-AChRs, mAb 35-AChRs, and synaptic sites. Blobs containing both α-Bgt-AChRs and mAb 35-AChRs are cyan, while regions containing both mAb 35-AChRs and synaptic vesicle antigen are yellow. Two generalizations that can be drawn from these images are (1) that surface patches containing both α-Bgt-AChRs and mAb 35-AChRs are usually perisynaptic (e.g., Fig. 9*J,L,M*), and (2) that both α-Bgt-AChRs and mAb 35-AChRs are occasionally found in clusters at the margin of synaptic boutons. It is more common to find such clusters with mAb 35-AChRs alone (e.g., Fig. 9*K*, arrow), but in adults, more so than in embryos, we also find occasional synaptic clusters containing both mAb 35-AChRs and α- Bgt-AChRs (e.g., Fig. 9*J*, arrow).

The major findings resulting from a comparison of the distribution of α-Bgt-AChRs, mAb 35-AChRs, and synaptic sites are similar in adult and embryonic neurons: a significant majority of both classes of receptors are extrasynaptic, and very often perisynaptic. At both stages, mAb 35-AChRs are found in small clusters that lie at the margin of some synaptic sites. The principal difference between the two stages relates to the overlap between α-Bgt-AChRs and synaptic sites; in adults, but not in embryos, we found a small population of α-Bgt-AChR clusters at the margin of synaptic sites.

Discussion

The presence of mAb 35-AChRs and of α-Bgt-AChRs in virtually all embryonic neurons complements previous work suggesting that both classes of AChRs are expressed in most or all neurons in the ciliary ganglion (Jacob and Berg, 1988; Jacob, 1991; Corriveau and Berg, 1993). Thus, there is little or no cellular diversity within the ganglion in the embryo with regard to the expression of these two major AChR classes, and our results suggest that this is true in the adult as well (Table 3).

Our finding that α-Bgt-AChRs are principally extrasynaptic both in embryonic and adult ciliary ganglia is consistent with previous studies of the distribution of α-Bgt-AChRs in this tissue. Electron microscopic examination of surface regions containing high concentrations of α-Bgt-AChRs show them to contain numerous small pseudodendrites and to lie beneath regions of the preganglionic calyx that lack synaptic vesicles (Jacob and Berg, 1983; Loring et al., 1985). The patches containing α-Bgt-AChRs (Fig. 4) presumably represent these regions, inasmuch as they appear to project from the neuronal surface. Individual patches may be composed of a number of smaller, punctate AChR clusters, each of which may be an individual patch of immunoperoxidase reaction as visualized by Jacob and Berg (1983). By reconstructing stacks of optical sections taken through the thickness of individual neurons, we have generated revealing views of the relationship between α-Bgt-AChR-rich membrane patches and synaptic sites: α-Bgt-AChR-patches are often located immediately adjacent to synaptic sites. In embryos, when ciliary neurons have calyceal endings, patches of α-Bgt-AChRs are surrounded, partially or completely, by SV2-bearing regions of the calyx. On adult neurons where the calyx is gone, the relationship is reversed: individual synaptic boutons are surrounded by one or more α-Bgt-AChR-rich patches. In the embryo, we rarely saw α-Bgt-AChR patches located more than a micrometer or two from the edge of a synaptic site, while in adults some α-Bgt-AChR-containing patches were not perisynaptic. The spatial relationship between α-Bgt-AChR-containing patches and synaptic sites can hardly have arisen randomly. We note that the pattern of α-Bgt-AChR-containing patches changes relatively little between embryonic and adult stages, at least judged qualitatively (compare Figs. 4 and 8*A,B*), as compared to a profound change in the arrangement of synaptic sites (compare Fig. 3 and Fig. 7). It is therefore possible that the sustained perisynaptic arrangement of many α-Bgt-AChR-containing patches is attributable to the presynaptic neuron, which "reads" the location of the patches and builds its release sites adjacent to them. It would be useful to know the order of appearance of α-Bgt-AChRs patches and release sites during development of the ganglion.

Patch-like regions of the neuronal surface that contain α-Bgt-AChRs also contain mAb 35-AChRs. Jacob et al. (1984) occasionally found clusters of mAb 35-AChRs in extrasynaptic regions containing "pseudodendrites," but only with the double-label experiments described here is it possible to say that these regions also contain α-Bgt-AChRs. Careful examination suggests, however, that there is heterogeneity within the patches: they are not invariably uniform in color in merged images (see insets in Figs. 6*G,H*, 9*G,H*), and thus the two AChR types may be found in distinct clusters within the patches. Immunochemical studies on ciliary ganglion extracts by Vernallis et al. (1993) suggest that α-Bgt and mAb 35 recognize largely distinct AChR classes, and thus we do not expect that the extensive overlap between α-Bgt-AChRs and mAb 35-AChRs results from α-Bgt and mAb 35/210 binding to the same AChR oligomer.

Only a small fraction of the detectable mAb 35-AChRs were found to be synaptic. This result is apparently not an artifact due to incomplete immunocytochemical staining of either synaptic boutons or of AChRs (see Results). A majority of mAb 35-AChRs are located in the patches they share with α-Bgt-AChRs, and these patches are almost exclusively perisynaptic. MAb 35-AChRs not located in patches were found in smaller clusters, a few of which are located at synaptic sites. The synaptic mAb 35-AChR-containing clusters are often located at the margin of regions of SV2 immunoreactivity, and it is natural to wonder whether active zones might also be located there. We suspect that the synaptic clusters of mAb 35-AChRs represent the same sites previously identified by Jacob et al. (1984) using immunoperoxidase techniques and electron microscopy. MAb 35-

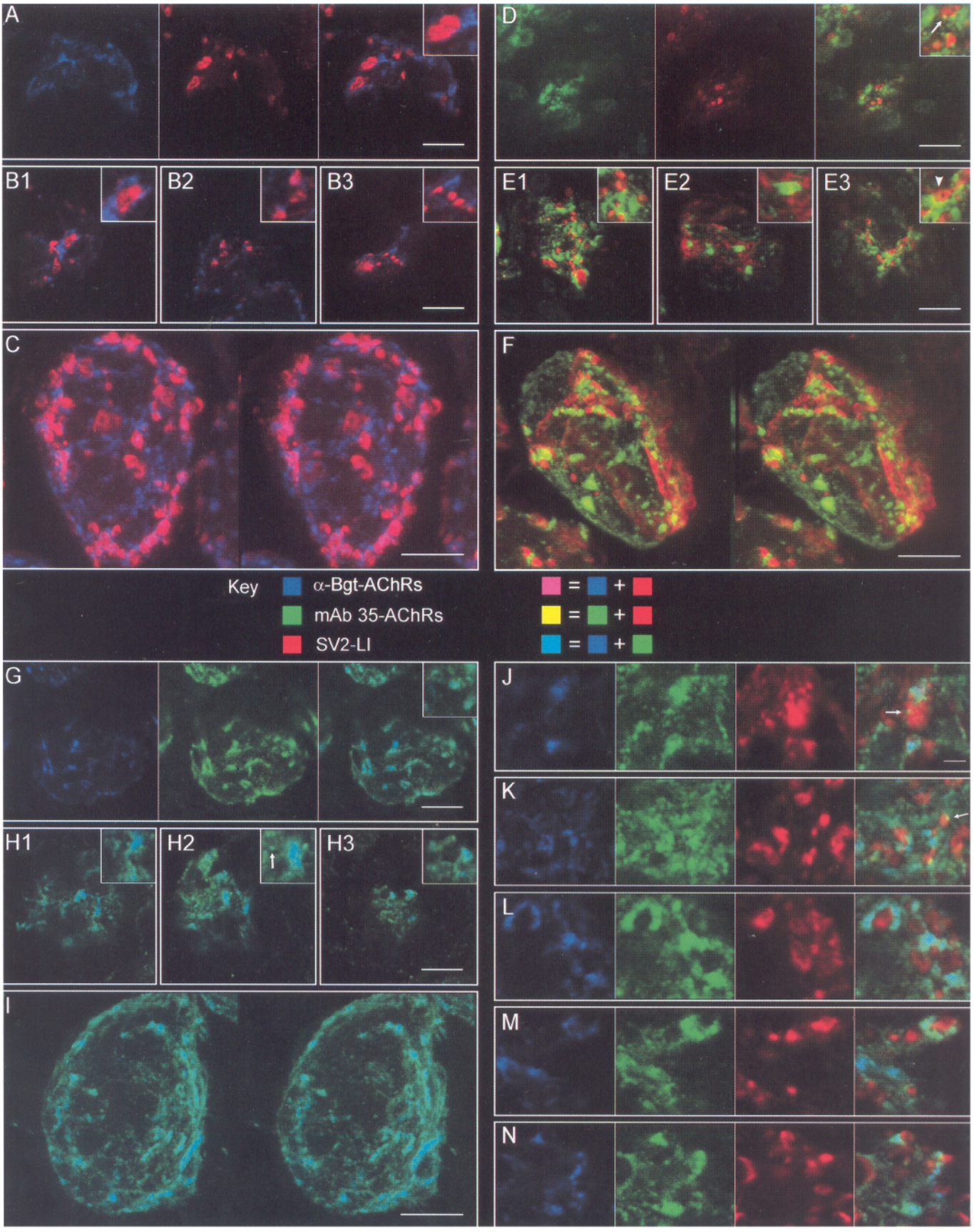
A
B1
B2
B3
C
D
E1
E2
E3
F
Key
α-Bgt-AChRs
mAb 35-AChRs
SV2-LI
=
+
G
H1
H2
H3
I
J
K
L
M
N

AChRs at these sites presumably underlie rapid excitatory synaptic transmission in the ganglion, but the subunit composition of these AChRs is not yet established. Recent findings from Berg and collaborators indicate that mAb 35 recognizes at least three classes of AChRs in the ganglion: (1) those containing α3, α5, and β4 subunits (but not β2 or α7; Conroy and Berg, 1995), (2) those containing α3, α5, β4, and β2 subunits (but not α7; Conroy and Berg, 1995), and (3) those containing none of the subunits known to be expressed in the ganglion as a whole (α3, α5, α7, β2, and β4) and likely to contain AChR subunits not yet identified by cloning (Pugh et al., 1995).

Synaptic clusters of mAb 35-AChRs account for only a small fraction of all the immunocytochemically demonstrable mAb 35-AChRs on the cell surface. As an order of magnitude estimate, we would estimate that no more than 10% of the mAb 35-AChRs we detect are located at synaptic sites on the basis of our experiments; it is possible that fewer than 1% of the mAb 35-AChRs are synaptic. This finding should be compared to the results of Jacob et al. (1984), who found that immunoperoxidase reaction product produced via the binding of mAb 35-HRP to its receptor was predominantly located at synapses, with only occasional patches of reaction product found extrasynaptically. One experimental difference between our study and that of Jacob et al. (1984) is that we visualized mAb 35-AChRs on formaldehyde-fixed neurons from embryonic day 19–21 ciliary ganglia, while they analyzed unfixed ganglia from embryonic day 16. However, we have repeated our confocal analysis on unfixed, 16 day ganglia, and find, again, that the majority of the mAb 35-AChRs detected are extrasynaptic. The difference between our results and those by Jacob et al. (1984) may relate to differences in the method of analysis (EM vs LSCM) and the fact that in neither instance is the measurement of synaptic/extrasynaptic distribution quantitatively reliable. We think it likely that the LSCM analysis of immunofluorescently labeled AChRs is generally more sensitive than the peroxidase technique. For example, we have recently discovered a class of small AChR clusters on the surface of frog cardiac ganglion neurons that were previously undetected by electron microscopy using the same mAbs and the ABC immunoperoxidase technique (Wilson and Sargent, 1994). Thus, it is possible that the sites of highest density of mAb 35-AChRs are synaptic, while large expanses of membrane in pseudodendrite-rich areas contain mAb 35-AChRs at a lower density. A consequence of the enrichment of membrane in these regions is that they contain many more AChRs than do synaptic sites.

Our results are somewhat comparable to the findings of Loring and Zigmond (1987), in which AChRs in embryonic ciliary ganglion were visualized with ^{125}I-neuronal bungarotoxin (n-Bgt) and electron microscopic autoradiography. Neuronal-bungarotoxin blocks synaptic transmission in the ciliary ganglion (Chiappinelli, 1983) and recognizes an AChR also recognized by mAb 35 (Halvorsen and Berg, 1987). Loring and Zigmond (1987) found that the grain density at synaptic sites was considerably higher than that elsewhere on the neuronal surface. However, synaptic sites only accounted for 38% of total grains counted in their study. A majority of the autoradiographic grains were found in extrasynaptic areas, most of them in regions containing pseudodendrites. Thus, it is possible that most of the n-Bgt binding sites are extrasynaptic, owing to the substantial enrichment of membrane in patches containing pseudodendrites.

Synaptic transmission in the ciliary ganglion begins in the fifth day after fertilization, and by E20, synapses on both ciliary and choroid neurons are well developed (reviewed in Dryer, 1994). One might still propose, however, that synapses at E20 represent an intermediate stage in a process of maturation that results ultimately in the complete loss of extrasynaptic AChRs. Our results in adults suggest that extrasynaptic AChRs are a lasting feature of ciliary ganglion cells, and it is worthwhile

←

Figure 9. Comparison of the distribution of α-Bgt-AChRs, mAb 35-AChRs, and SV2 immunoreactivity in adult ciliary ganglion neurons. Each molecule is consistently rendered a different primary color, according to the key (*center*). Colocalization of two colors will be revealed by magenta (blue plus red), yellow (green plus red), or cyan (blue plus green), as indicated in the key. The first three quadrants (*A–C, D–F,* and *G–I*) display the results of pair-wise comparisons, while the last quadrant (*J–N*) displays the results of triple label experiments. *A–C* show the relative location of α-Bgt-AChRs (blue) and synaptic sites (SV2 immunoreactivity, red). *A* shows the distribution of α- Bgt-AChRs in the *left panel,* of synaptic sites in the *middle panel,* and of both in the right panel, all for an optical section that grazes the upper surface of an adult ciliary ganglion neuron. The *right panel* in *A,* and its *inset,* shows that patch-like regions containing α-Bgt-AChRs are adjacent to synaptic sites and often partially surround them. Areas of overlap are rare. Similar results are shown in *B,* which shows three additional examples of merges (as in *A, right panel*). *C* shows a stereopair that demonstrates the perisynaptic nature of the patches of some of the α-Bgt-AChRs. Regions of evident overlap at the margins of the neuron are only apparent, since the spatial resolution of the laser scanning confocal microscope in the z direction is less than that in the x and y directions. *D–F* show the relative location of mAb 35-AChRs (green) and synaptic sites (SV2 immunoreactivity, red). *D* shows the distribution of mAb 35-AChRs in the left panel, of synaptic sites in the *middle panel,* and of both in the *right panel,* all for an optical section that grazes the upper surface of a ciliary ganglion neuron. The *right panel in D,* and its *inset,* shows that some overlap exists between surface regions rich in mAb 35-AChRs and those rich in synaptic vesicles (*arrow*). While the larger, patch-like areas containing mAb 35-AChRs tend to be extrasynaptic, smaller, punctate clusters of mAb 35-AChRs sometimes overlap with synaptic sites, indicated by the presence of yellow spots in the merged image (and *inset*) and in additional examples (*E*). A second type of colocalization where diffuse mAb 35-AChRs are found at a synaptic site (*E3, arrowhead*). *F* shows a stereopair illustrating that most of the mAb 35-AChRs are extrasynaptic and are green, as opposed to yellow, in merged images. *G–I* show pair-wise shows the relative location of α-Bgt-AChRs (blue) and mAb 35-AChRs (green). *G* shows the distribution of α-Bgt-AChRs in the left panel, of mAb 35-AChRs in the *middle panel,* and of both in the *right panel,* all for an optical section that grazes the upper surface of a ciliary ganglion neuron. The *right panel* in *G,* and its inset, shows that the patch-like regions containing α-Bgt-AChRs also contain mAb 35-AChRs and are rendered cyan in the color merge (see *inset*). Similar results are shown in *H,* which shows three additional examples of merges (as in *G, right panel*). Numerous green (mAb 35-AChRs) spots appear on the neuronal surface unaccompanied by detectable concentration of α-Bgt-AChRs (*H2, inset, arrow*). *I* shows a stereopair that demonstrates extensive overlap between α-Bgt-AChRs and mAb 35-AChRs. Most of the regions containing α-Bgt-AChRs also have mAb 35-AChRs (cyan), while there are many mAb 35-AChR clusters that lack α-Bgt-AChRs (green). *J–N* show the results of triple label experiments and depict, at high magnification, regions of the surface of individual neurons, taken from optical sections that graze the neuronal surface. The *first three panels* show the distribution of α-Bgt-AChRs, mAb 35-AChRs, and synaptic sites in common fields, while the *right panel* shows a color merge of all three distributions. The bulk of the α-Bgt-AChRs and the mAb 35-AChRs are found together in large, extrasynaptic patches (cyan). Some of the small mAb 35-AChR clusters that lie adjacent to these patches are synaptic (*K, arrow*) as are other small clusters that contain both mAb 35- and α-Bgt-AChRs (*J, arrow*). All scale bars in *A–I* are 10 μm. Scale bars in *A, D,* and *G* are for all images in the relevant quadrants except the stereopairs, which have their own scale bar. *Insets* in *B, E,* and *H* are magnified two times and measure 6 μm by 6 μm. Scale bar in *J* is 2.5 μm and is for *J–N.*

considering what their function might be. A possible clue is provided by the location of these AChRs. The extrasynaptic patches that contain both mAb 35-AChRs and α-Bgt-AChRs bear a striking spatial relationship to synaptic sites: all (embryo) or many (adult) are perisynaptic. The AChRs in these patches may respond to neurotransmitter released from nearby active zones, which may be only 1–2 μm distant. While the presence of acetylcholinesterase on the neuronal surface (Fumagalli et al., 1982) would be expected to reduce the effective range of released ACh, it is possible that increased rates of stimulation, such as might occur during a high frequency burst of preganglionic action potentials, might allow released ACh to gain access to extrasynaptic AChRs. However, Zhang et al. (1994) have shown that α-Bgt-AChRs desensitize rapidly to the applications of agonist, and it is unclear whether these receptors could produce much current if activated by ACh released from noncolocalized terminals or from other sources in the body. However, Vijayaraghavan et al. (1992) showed that activation of these receptors can lead to changes in intracellular calcium concentration in ciliary ganglion neurons unaccompanied by measurable membrane current. These receptors may not function to regulate the membrane potential of the cell but rather to regulate other cellular functions via second messenger systems. Indeed, Vijayaraghavan et al. (1995) recently showed that activation of these AChRs by nicotine leads to the release of arachidonic acid from intracellular stores. It would be particularly useful to learn under what conditions naturally released transmitter can activate such second messenger systems.

References

Buckley K, Kelly RB (1985) Identification of a transmembrane glycoprotein specific for secretory vesicles of neural and endocrine cells. J Cell Biol 100:1284–1294.

Chiappinelli VA (1983) Kappa-bungarotoxin: a probe for the neuronal nicotinic receptor in the avian ciliary ganglion. Brain Res 277:9–21.

Conroy WG, Berg DK (1995) Neurons can maintain multiple classes of nicotinic acetylcholine receptors distinguished by different subunit compositions. J Biol Chem 270:4424–4431.

Conroy WG, Vernallis AB, Berg DK (1992) The alpha5 gene product assembles with multiple acetylcholine receptor subunits to form distinctive receptor subtypes in brain. Neuron 9:679–691.

Corriveau R, Berg DK (1993) Coexpression of multiple acetylcholine receptor genes in neurons: quantification of transcripts during development. J Neurosci 13:2662–2671.

Couturier S, Bertrand D, Matter J-M, Hernandez M-C, Bertrand S, Millar N, Valera S, Barkas T, Ballivet M (1990) A neuronal nicotinic acetylcholine receptor subunit (alpha7) is developmentally regulated and forms a homo-oligomeric channel blocked by alpha-BTX. Neuron 5:847–856.

Dryer SE (1994) Functional development of the parasympathetic neurons of the avian ciliary ganglion: a classical model system for the study of neuronal differentiation and development. Prog Neurobiol 43:281–322.

Fumagalli L, DeRenzis G (1980) Extrasynaptic localization of α- bungarotoxin receptors in the rat superior cervical ganglia. Neurochem Int 6:355–364.

Fumagalli L, Del Fa A, Olivieri-Sangiacomo C (1982) Surface AChE in the chick ciliary ganglion neurons: ultrastructural localization and possible relations to α bungarotoxin receptors. Neurochem Int 4:15–21.

Giloh H, Sedat JW (1982) Fluorescence microscopy: reduced photobleaching of rhodamine and fluorescein protein conjugates by n-propyl gallate. Science 217:1252–1255.

Glantz SA (1992) Primer of biostatistics. New York: McGraw-Hill.

Hall ZW, Sanes JR (1993) Synaptic structure and development: the neuromuscular junction. Neuron 10:99–121.

Halvorsen SW, Berg DK (1987) Affinity labeling of neuronal acetylcholine receptor subunits with an alpha-neurotoxin that blocks receptor function. J Neurosci 7:2547–2555.

Haselbeck RC, Conroy WG, Romano SJ, Berg DK (1994) Expression of neuronal acetylcholine receptor genes in transfected HEK-293 cells. Soc Neurosci Abstr 20:1130.

Hess A (1965) Developmental changes in the structure of the synapse on the myelinated cell bodies of the chicken ciliary ganglion. J Cell Biol 25:1–19.

Jacob MH (1991) Acetylcholine receptor expression in developing chick ciliary ganglion neurons. J Neurosci 11:1701–1712.

Jacob MH, Berg DK (1983) The ultrastructural localization of alpha-bungarotoxin binding sites in relation to synapses on chick ciliary ganglion neurons. J Neurosci 3:260–271.

Jacob MH, Berg DK (1987) Effects of preganglionic denervation and postganglionic axotomy on acetylcholine receptors in the chick ciliary ganglion. J Cell Biol 105:1847–1854.

Jacob MH, Berg DK (1988) The distribution of acetylcholine receptors in chick ciliary ganglion neurons following disruption of ganglionic connections. J Neurosci 8:3838–3849.

Jacob MH, Berg DK, Lindstrom JM (1984) Shared antigenic determinants between *Electrophorus* acetylcholine receptor and a synaptic component on chicken ciliary ganglion neurons. Proc Natl Acad Sci USA 81:3223–3227.

Jacob MH, Lindstrom JM, Berg DK (1986) Surface and intracellular distribution of a putative neuronal nicotinic acetylcholine receptor. J Cell Biol 103:205–214.

Landmesser L, Pilar G (1972) The onset and development of transmission in the chick ciliary ganglion. J Physiol (Lond) 222:691–713.

Loring RH, Zigmond RE (1987) Ultrastructural distribution of ^{125}I-toxin F binding sites on chick ciliary neurons: synaptic localization of a toxin that blocks ganglionic nicotinic receptors. J Neurosci 7:2153–2162.

Loring RH, Chiappinelli VA, Zigmond RE, Cohen JB (1984) Characterization of a snake venom neurotoxin which blocks nicotinic transmission in the avian ciliary ganglion. Neuroscience 11:989–999.

Loring RH, Dahm LM, Zigmond RE (1985) Localization of α-bungarotoxin binding sites in the ciliary ganglion of the embryonic chick: an autoradiographic study at the light and electron microscopic level. Neuroscience 14:645–660.

McGehee DS, Role LW (1995) Physiological diversity of nicotinic acetylcholine receptors expressed by vertebrate neurons. Annu Rev Physiol 57:521–546.

Parzen E (1960) Modern probability theory and its applications. New York: Wiley.

Pugh PC, Corriveau RA, Conroy WG, Berg DK (1995) Novel subpopulation of neuronal acetylcholine receptors among those binding alpha-bungarotoxin. Mol Pharmacol 47:717–725.

Ravdin PM, Berg DK (1979) Inhibition of neuronal acetylcholine sensitivity by alpha-toxins from *Bungarus multicinctus* venom. Proc Natl Acad Sci USA 76:2072–2076.

Saedi MS, Anand R, Conroy WG, Lindstrom J (1990) Determination of amino acids critical to the main immunogenic region of intact acetylcholine receptors by *in vitro* mutagenesis. FEBS Lett 267:55–59.

Sargent PB (1983) The number of synaptic boutons terminating on *Xenopus* cardiac ganglion cells is directly correlated with cell size. J Physiol (Lond) 343:85–104.

Sargent PB (1993) The diversity of neuronal nicotinic acetylcholine receptors. Annu Rev Neurosci 16:403–443.

Sargent PB (1994) Double-label immunofluorescence with the laser scanning confocal microscope using cyanine dyes. Neuroimage 1:288–295.

Sargent PB, Pang DZ (1988) Denervation alters the size, number, and distribution of clusters of acetylcholine receptor-like molecules on frog cardiac ganglion neurons. Neuron 1:877–886.

Sargent PB, Pang DZ (1989) Acetylcholine receptor-like molecules are found in both synaptic and extrasynaptic clusters on the surface of neurons in the frog cardiac ganglion. J Neurosci 9:1062–1072.

Sargent PB, Wilson HL (1994) Distribution of nicotinic acetylcholine receptor subunit immunoreactivities on the surface of chick ciliary ganglion neurons. Proceedings of the International Symposium on Nicotine (Satellite Symposium of the XIIth International Congress of Pharmacology, Montreal, Canada), P1 (abstract). Basel: Birkhäuser.

Schoepfer R, Conroy WG, Whiting P, Gore M, Lindstrom J (1990) Brain alpha-bungarotoxin binding protein cDNAs and MAbs reveal subtypes of this branch of the ligand-gated ion channel gene superfamily. Neuron 5:35–48.

Smith MA, Margiotta JF, Berg DK (1983) Differential regulation of acetylcholine sensitivity and α-bungarotoxin-binding sites on ciliary neurons in cell culture. J Neurosci 3:2395–2402.

Smith MA, Margiotta JF, Franco A, Lindstrom JM, Berg DK (1986) Cholinergic modulation of an acetylcholine receptor-like antigen on the surface of chick ciliary ganglion neurons in cell culture. J Neurosci 6:946–953.

Tzartos SJ, Lindstrom JM (1980) Monoclonal antibodies used to probe acetylcholine receptor structure: localization of the main immunogenic region and detection of similarities between subunits. Proc Natl Acad Sci USA 77:755–759.

Tzartos S, Hochschwender S, Vasquez P, Lindstrom J (1987) Passive transfer of experimental autoimmune myasthenia gravis by monoclonal antibodies to the main immunogenic region of the acetylcholine receptor. J Neuroimmunol 15:185–194.

Tzartos SJ, Rand DE, Einarson BL, Lindstrom JM (1981) Mapping of surface structures of *Electrophorus* acetylcholine receptor using monoclonal antibodies. J Biol Chem 256:8635–8645.

Vernallis AB, Conroy WG, Berg DK (1993) Neurons assemble acetylcholine receptors with as many as three kinds of subunits while maintaining subunit segregation among receptor subtypes. Neuron 10:451–464.

Vijayaraghavan S, Pugh PC, Zhang Z-W, Rathouz MM, Berg DK (1992) Nicotinic receptors that bind alpha-bungarotoxin on neurons raise intracellular free Ca^{2+}. Neuron 8:352–363.

Vijayaraghavan S, Huang B, Blumenthal EM, Berg DK (1995) Arachidonic acid as a possible negative feedback inhibitor of nicotinic acetylcholine receptors on neurons. J Neurosci 15:3679–3687.

Wilson HL, Sargent PB (1994) Effects of denervation upon acetylcholine receptor clusters in autonomic neurons as determined by quantitative laser scanning confocal microscopy. Soc Neurosci Abstr 20: 1139.

Zhang Z-W, Vijayaraghavan S, Berg DK (1994) Neuronal acetylcholine receptors that bind α-bungarotoxin with high affinity function as ligand-gated ion channels. Neuron 12:167–177.